Mutant FUS induces chromatin reorganization in the hippocampus and alters memory processes

Laura Tzeplaeff, Jonathan Seguin, Stéphanie Le Gras, Salim Megat, Brigitte Cosquer, Damien Plassard, Stéphane Dieterlé, Isabel Paiva, Gina Picchiarelli, Charles Decraene, et al.

Mutant FUS induces chromatin reorganization in the hippocampus and alters memory processes

Running title: Epigenetic dysfunctions in FUS-related diseases

Laura Tzeplaeff [1,2,3], Jonathan Seguin [1,2], Stéphanie Le Gras [4], Salim Megat [3], Brigitte Cosquer [1,2], Damien Plassard [4], Stéphane Dieterlé [3], Isabel Paiva [1,2], Gina Picchiarelli [3], Charles Decraene [1,2], Rafael Alcala-Vida [1,2], Jean-Christophe Cassel [1,2], Karine Merienne [1,2], Luc Dupuis [3*#] and Anne-Laurence Boutillier [1,2*#].

[1] Université de Strasbourg, Laboratoire de Neuroscience Cognitives et Adaptatives (LNCA), Strasbourg, France
[2] CNRS, UMR 7364, Strasbourg 67000, France
[3] Université de Strasbourg, INSERM, UMR-S1118, Strasbourg, France
[4] Université de Strasbourg, CNRS UMR 7104, INSERM U1258, GenomEast Platform, Institut de Génétique et de Biologie Moléculaire et Cellulaire (IGBMC), Université de Strasbourg, Illkirch, France

* Equal contribution

Corresponding authors:

Anne-Laurence Boutillier: laurette@unistra.fr
Université de Strasbourg, Cnrs, UMR7364, Laboratoire de Neuroscience Cognitives et Adaptatives (LNCA), 12 rue Goethe, 67000 Strasbourg, France

Luc DUPUIS, ldupuis@unistra.fr
Université de Strasbourg, Inserm, UMR-S1118, Centre de Recherches en Biomédecine de Strasbourg, CRBS, 1 rue Eugene Boeckel, 67000 Strasbourg, France

e-mail addresses :
Laura Tzeplaeff: laura.tzeplaeff@gmail.com
Jonathan Seguin: seguin.jonathan@gmail.com
Stephanie Le Gras: slegras@igbmc.fr
Salim Megat: salim.megat@inserm.fr

Brigitte Cosquer: brigitte.cosquer@unistra.fr
Damien Plassard: plassard@igbmc.fr
Stéphane Dieterle: stephane.dieterle@orange.fr
Isabel Paiva: paivadecastro@unistra.fr
Gina Picchiarelli: gina.picchiarelli@free.fr
Charles Decraene: charles.decraene@unistra.fr
Rafael Alcala-Vida: ralcala@umh.es
Jean-Christophe Cassel: jcassel@unistra.fr
Karine Merienne: karine.merienne@unistra.fr
Luc Dupuis: ldupuis@unistra.fr
Anne-Laurence Boutillier: laurette@unistra.fr

Abbreviations

AD: Alzheimer's disease
ALS: Amyotrophic Lateral Sclerosis
BP: Biological process
CA1: Cornu Ammonis 1
CC: Cellular component
ChIP: Chromatin Immunoprecipitation
CNS: Central Nervous System
DAVID: Database for Annotation, Visualization and Integrated Discovery
ETS: E Twenty Six
FDR: False Discovery Rate
FET family: the name derives from the first letters of FUS, EWSR1, and TAF15
FANS: Fluorescent Activated Nuclei Sorting
FUS: Fused in Sarcoma
FTD: Fronto-Temporal Dementia
GO: Gene Ontology
GREAT: Genomic Regions Enrichment of Annotations Tool
HC: Home Cage
HDAC: Histone Deacetylase
HMEG: Histone Mark Enriched Gene
KEGG: Kyoto encyclopedia of Genes and Genomes
MWM: Morris Water Maze
NLS: Nuclear Localisation Signal
SERE: Simple Error Ratio Estimate
SICER: Spatial clustering for identification of ChIP-enriched regions

STRING: Search Tool for Recurring Instances of Neighbouring Genes

SWI/SNF : SWItch/Sucrose Non-Fermentable

TSS: Transcription Start Site

Abstract

Cytoplasmic mislocalization of the nuclear *Fused in Sarcoma* (FUS) protein is associated to amyotrophic lateral sclerosis (ALS) and frontotemporal dementia (FTD). Cytoplasmic FUS accumulation is recapitulated in the frontal cortex and spinal cord of heterozygous *Fus*$^{\Delta NLS/+}$ mice. Yet, the mechanisms linking FUS mislocalization to hippocampal function and memory formation are still not characterized. Herein, we show that in these mice, the hippocampus paradoxically displays nuclear FUS accumulation. Multi-omic analyses showed that FUS binds to a set of genes characterized by the presence of an ETS/ELK-binding motifs, and involved in RNA metabolism, transcription, ribosome/mitochondria and chromatin organization. Importantly, hippocampal nuclei showed a decompaction of the neuronal chromatin at highly expressed genes and an inappropriate transcriptomic response was observed after spatial training of *Fus*$^{\Delta NLS/+}$ mice. Furthermore, these mice lacked precision in a hippocampal-dependent spatial memory task and displayed decreased dendritic spine density. These studies shows that mutated FUS affects epigenetic regulation of the chromatin landscape in hippocampal neurons, which could participate in FTD/ALS pathogenic events. These data call for further investigation in the neurological phenotype of FUS-related diseases and open therapeutic strategies towards epigenetic drugs.

Key words

ALS/FTD, FUS, hippocampus, histone modifications, neuronal chromatin, spatial memory

1. Introduction

FUS is a ubiquitously expressed RNA binding protein that has pleiotropic roles in RNA metabolism, including transcription, splicing, mRNA transport, microRNA and circRNA biogenesis and mRNA translation (Lagier-Tourenne *et al.*, 2010; Lagier-Tourenne *et al.*, 2012). As a protein involved in gene expression, FUS is highly enriched in the nucleus, yet shuttles between nucleus and cytoplasm. FUS carries a C-terminal PY-NLS allowing nuclear entry and is subject to post-translational modifications regulating nuclear import and function. Abnormalities in FUS subcellular localization are found in multiple neurodegenerative diseases. First, germline mutations in FUS are a cause of young onset amyotrophic lateral sclerosis (ALS), with rapid disease progression, and the most severe *FUS* mutations lead to truncation of the C-terminal amino-acids of FUS comprising the nuclear localization signal. FUS mutations lead to FUS pathological aggregates, located in the cytoplasm, but also in nuclear inclusions (Schwartz *et al.*, 2014)(Baumer *et al.*, 2010). FUS aggregates are also

found in a large subset of patients with FTD, along with other proteins of the FET family (Urwin *et al.*, 2010). In addition, FUS is mislocalized in the cytoplasm, but not aggregated, in most ALS cases, but also in other neurodegenerative diseases in the absence of germline FUS mutation (Tyzack *et al.*, 2019). FUS mutation has broad effects on neuronal functions as heterozygous mice with a knock-in mutation of *Fus* leading to its C-terminal truncation and accumulated cytoplasmic FUS led to cortical neuronal hyperactivity and inhibitory synaptic defects, causing related behavioral phenotype (Scekic-Zahirovic *et al.*, 2021).

Several independent lines of evidence suggest an important role for FUS in the hippocampus. First, FUS pathology is prominent in the hippocampus of FTD-FUS patients (Armstrong *et al.*, 2011a, b; Baborie *et al.*, 2011; Mackenzie *et al.*, 2011). Further, ablation of *Fus* in outbred mice leads to prominent hippocampal vacuolation (Kino *et al.*, 2015), and *Fus* knockdown in the hippocampus leads to neuronal death and behavioral phenotypes (Udagawa *et al.*, 2015; Fujii *et al.*, 2005). In addition, human wild-type FUS expression leads to defects in fear conditioning, decreased LTP and abnormal dendritic spine morphology in the hippocampus (Ho *et al.*, 2019). Last, FUS appears required for spine formation and maturation, AMPA receptors expression (Udagawa *et al.*, 2015) or adult neurogenesis (Ishigaki *et al.*, 2017), all critically involved in hippocampal function. However, despite this evidence, the mechanisms linking FUS mislocalization and/or aggregation, to hippocampal function and memory formation are still not characterized.

Here, we hypothesize that mutant FUS may alter nuclear function in chromatin remodeling processes that occur during memory formation. Indeed, FUS is involved in multiple steps of gene expression including transcription (Schwartz *et al.*, 2012), alternative splicing, and interacts and modulates activity of a number of chromatin remodeling enzymes, including HDAC1 (Wang *et al.*, 2013), SWI/SNF (Linden *et al.*, 2019) and CBP/p300 (Wang *et al.*, 2008). In addition, several studies observed that manipulation of FUS levels in cellular models was able to alter histone post-translational modifications (Cobos *et al.*, 2019; Tibshirani *et al.*, 2014; Ward *et al.*, 2014). Furthermore, recent literature evidence that specific epigenetic changes driving activity-dependent transcription promotes the enhancement and plasticity of neural circuits underlying learning and memory processes (Campbell and Wood, 2019; Yap and Greenberg, 2018; Marco *et al.*, 2020; Fernandez-Albert *et al.*, 2019). Pathological deregulation of FUS nuclear functions might thus interfere with such processes. We investigated this possibility in a heterozygous FUS truncation ($Fus^{\Delta NLS/+}$) knock-in mouse model. This mouse model recapitulates many pathological hallmarks observed in ALS-*FUS* patients, such as cortical FUS cytoplasmic mislocalization, accompanied by motor deficit and motor neuron degeneration at the age of 20 months

(Scekic-Zahirovic *et al.*, 2017; Scekic-Zahirovic *et al.*, 2016). Additionally, 10-month-old *Fus*$^{\Delta NLS/+}$ mice showed impaired performance in several hippocampal-dependent behavioral tests and mutant FUS-induced cognitive dysfunctions may actually appear earlier.

Herein, we observed that a substantial fraction of nuclear FUS carried the truncating mutation in heterozygous mutant knock-in mice in their hippocampus. We further established that FUS binds the chromatin at the TSS of many genes carrying ETS-transcription factor binding sites, and that this binding of FUS is paradoxically increased at its genomic binding sites in *Fus* mutant mice. This was associated with active histone marks enrichment at highly expressed genes, at a large-scale, mainly extending the FUS genomic binding sites. Importantly, these large-scale epigenetic alterations were accompanied by prominent alterations in learning-induced transcriptional changes and significant defects in hippocampal dependent memory in mutant mice. Thus, our results suggest that the truncation of FUS NLS domain does not abolish nuclear import of the mutant protein in hippocampal adult neurons but rather leads to a nuclear gain-of-function with direct transcriptional effects (including on ETS-regulated target genes), large scale chromatin remodeling, that alter the neuronal response upon solicitation such as activity-induced transcription and learning and memory processes.

2. Material and methods

2.1. Animals

Experimental protocols and animal care were in compliance with the institutional guidelines (council directive 87/848, October 19, 1987, Ministère de l'agriculture et de la Forêt, Service Veterinaires de la Santé et de la Protection Animale) and international laws (directive 2010/63/UE, February 13, 2013, European Community) and policies APAFIS: 11229 (RôledeFUSdanslarégul_2017091118178028_v4).

Wild type and heterozygous *Fus*$^{\Delta NLS/+}$ mice in C57/BL6 genetic background were generated as described previously (Scekic-Zahirovic *et al.*, 2017) and bred and housed in the animal facility of the Laboratory of Cognitive and Adaptative Neuroscience (LNCA) of Strasbourg.

Mice were housed in group under a 12 light/dark cycle (light on at 7:00 a.m.), in a temperature and humidity-controlled room (22 ± 2 °C; 50% ± 5 humidity) with *ad libitum* access to food and water. For behavioral test, mice were single housed one week prior the test and habituated to handling 5 min a day during 3 days.

2.2.1. Morris water maze

Wild type and heterozygous *Fus*$^{\Delta NLS/+}$ mice of 4 months of age were trained to performed the hidden-platform version of the spatial Morris Water Maze for 5 consecutive days (n=11 animal per genotype). In a room, a circular pool (diameter 160 cm and height 60 cm) is located in the center and is surrounded by distal visual cues made of different shapes and colors on the walls. To habituate the mice to the pool and the platform rule, the pool is filled with few cm of water (21°C) and a visible platform is located in the NW quadrant (diameter 10 cm, 1cm above the surface). Starting from the middle of the pool, mice have 60s to find the platform, if not, they are gently brought there. After 10s on the platform, mice are brought back to their home cage. Then, the pool is filled with water up to 20 cm below the border so that mice can see the visual cues on the walls. The platform is placed 1cm below the surface and the water is opacified with Meudon white powder (about 1.5 g/L). Before acquisition, mice performed a 2 min forced swim (no platform), starting from the middle of the pool, to make sure they can all swim and complete the test. On the next days, mice were trained for 5 consecutive acquisition days to find the spatial position of the hidden platform located in the SE quadrant. Mice were trained with 4 trials a day, in group of 3, with an intertrial interval of 2-5 min and a maximum duration of the test of 60s. If not completed on time, mice were guided to the platform. Mice are left 10s on the platform before brought back in the home cage. Animals were starting each trial from each of the 4 cardinal points (North (N), East (E), South (S), and West (W)) from the edge of the pool, facing the wall. The sequence of the starting point was randomized each day. Mice were tested for memory retention on day 5, 24h after last training to test recent memory, and 30 days after last training to test remote memory (duration of the test 60s). At the end of the 24h memory retention, the Atlantis platform was brought to its original position, to avoid memory extinction processes and mice are further trained for the 5th day of acquisition as previous ones. For retention test, the platform was removed and the pool was virtually separated in 4 quadrants (SE, NE, NW, SW). Data and heat maps were collected by the ANY-maze (Ugo Basile) video tracking system. Average speed, latency and distance travelled to reach the SE target platformed were analyzed during acquisition. Time spent in the different quadrants, average distance from the target platform and the crossing annulus were analyzed during memory retention tests.

2.2.2. Analyses of MWM data

Data collected during the acquisition and during the different probe trials are presented as mean ± standard error of the mean (SEM). Values of $p < 0.05$ were considered significant and are noted in the text. Graphics and statistical analyses were performed using GraphPad Prism 8 (GraphPad, CA). Performances recorded during acquisition (latency, distance and mean speed) were evaluated using repeated two-way ANOVA considering the factors of

“genotype” (WT vs FUS) and “day” (1–5) and followed by Šidák correction for multiple comparisons. Mean time spent in the different quadrants (Target or favorite adjacent) were analyzed using two-way ANOVA with Šidák correction for multiple comparisons. Mean distance to platform was analyzed with the unpaired t test and the number of crossing annulus with the non-parametric unpaired Man-Whitney rank test. The time spent in quadrant was also compare to chance (i.e., 15 s) with the one sample t test.

2.3.1. Western blotting

Total tissues, of dorsal hippocampi (n=6 animal per genotype) were finely chopped on ice with a razor blade, and homogenized in Laemmli buffer (Biorad, Ref: 161-0747). Tissues were sonicated for 15 s, twice (ultrasonic processor, power 40%) followed by heating at 70°C for 10 min. Lysates were centrifuged at 14,000 g for 5 min. Protein concentration was quantified using the Qubit and supernatant was stored at –20°C before use. Equal amounts of protein were loaded on Midi-PROTEAN TGX Stain□Free™ Precast Gels (26 wells, 4–20%, Bio□Rad), transferred onto a nitrocellulose membrane (BioRad) using a semi-dry Transblot Turbo transfer system (BioRad). Membranes were blocked 1h with 5% non-fat milk in wash buffer (3% NaCL 5M, 0.05% Tween 20 and 5% Tris pH 7.4), and were then incubated overnight in blocking solution with the following primary antibodies: rabbit anti-FUS 1:5000 (Bethyl, Ref: A300-293A, Lot: A300-293A-5), rabbit anti-Actin 1:1000 (Abcam, Ref: A2066-100UL, Lot: 106M4770V), all diluted in blocking solution. The next day, membranes were washed three times and incubated with horseradish peroxidase (HRP)-labeled secondary antibodies goat anti-rabbit 1:10000 (Jackson, Ref: 111-035-003, Lot: 107487) in blocking solution. Bands showing the specific proteins were revealed with chemiluminescence (Biorad, Clarity Western ECL substrate, Ref: 170-5061) using the Molecular Imager Chemidoc Touch Imaging System (Biorad) as detection system and total protein as loading controls.

2.3.2. Quantification of protein on Western blot

Stain□free imaging allowed for the normalization of each protein bands to the total amount of protein with the ImageLab software (Biorad). Results in *Fus* mice were normalized to the relative amounts of proteins in WT mice (arbitrarily set at 1). Data are presented as mean ± standard error of the mean (SEM). Values of $p < 0.05$ were considered significant. Graphics and statistical analyses were performed using GraphPad Prism 8 (GraphPad, CA). Genotypes were compared using the unpaired two tailed *t-test.*

2.3.3. Western blot of subcellular fractionations

Nuclear and cytoplasmic fractions were prepared from frozen dorsal hippocampi (n=6 animal per genotype) using the NE-PER® Nuclear and Cytoplasmic Extraction reagents (Thermo Scientific) according to the manufacturer. Protein concentration was quantitated using the BCA protein assay kit (Pierce). Western blots were performed as described above, using following primary antibodies: goat anti-FUS against the N-terminal part of protein (ProteinTech 11570; 1:1000) and rabbit anti-FUS against the C-terminal part of protein (Bethyl A300-294A, 1:10000) all diluted in 3% non-fat milk in PBS, followed by incubation with horseradish peroxidase (HRP)-labeled secondary antibodies anti-goat (Sigma A5420) and anti-rabbit (P.A.R.I.S. BI2407) diluted 1:5000 in PBS. Antibodies rabbit anti-HDAC1 (Bethyl A300-713A, 1:1000) and mouse anti sheep SOD1 (Merk 574597, 1:1000) were respectively used as loading control for nuclear and cytoplasmic fractions. Blots were analyzed with chemiluminescence (ECL; Luminata Forte Kit, Millipore WBLUF0500) using the Molecular Imager Chemidoc XRS (Biorad) as detection system. Results were analyzed as described above.

2.4. Brain perfusion for immunohistochemistry

Mice were deeply anesthetized with 0.1ml/10g Ketamine (Imalgène 1000) and Xylazine (Rompun 2%) (respectively 20% and 15% in NaCl 0,9%) and underwent a transcardial perfusion with PBS (0.1 M phosphate buffer saline) followed by cold 4% paraformaldehyde (PFA) in PBS. Brains were removed and fixed overnight in 4% PFA and subsequently merged in 30% sucrose solution at 4°C until the brain sank. Brains were cut with the cryostat into 30µm thick coronal sections in the whole hippocampal region. Sections were kept at 20°C in cryoprotectant (0.1 M PBS, 0.15 M NaCl, 30% (v/v) ethylene glycol, 30% (v/v) glycerol) until immunostaining.

2.5. Immunohistochemistry

Free floating brain sections were rinsed three times in PBS (0.25% Triton X-100 in PBS, 137 mM NaCl, 2.7 mM KCl, 10 mM Na2HPO4, 1.8 mM KH2PO4). For heat-induced epitope retrieval, floating sections were kept in sodium citrate (pH 6, 10 mM, 80°C, 30 min) and washed three times in 1XPBS. Sections were blocked in blocking solution (1XPBS with 0.5% Triton and 5% Horse serum) for 30 minutes and then incubated overnight (ON) in the following primary antibodies at 4°C: rabbit anti-FUS (ProteinTech, 1:1000) and mouse anti-NeuN (Millipore, 1:500) in PBS with Triton 0.1%. The next day, brain sections were rinsed and incubated at RT for 1h30 respectively with, donkey anti-rabbit Alexa 488-conjugated (Jackson 1:500) and donkey anti-mouse Alexa 594-conjugated (Molecular Probes, 10ug/ml) in PBS with Triton 0.1%. After three washes in 1XPBS, brain sections were incubated in Dapi diluted 1:1000 in 1XPBS for nuclei staining, washed two times in 1XPBS before drying and

mounting sections in Mowiol (Life Technologies; 1:10000), cover-slipped, and kept at 4°C for long storage.
Acquisitions were performed using a fluorescence microscope coupled with an ApoTome module (Zeiss).

2.6. RNA extraction

Mice that underwent a 3-day training in the MWM were killed 1h after the last training. Home-cage controls were killed at the same time. Half dorsal hippocampus of trained mice and their home cage (HC) control were chopped on ice with a razor blade before extraction of total RNA using the RNeasy Lipid Tissue Mini Kit (Qiagen).

2.7. RNA sequencing and analyses

Quality control, libraries and sequencing were processed by the GenomEast platform (IGBMC, Strasbourg). RNA quality was measured using the Agilent Bioanalyzer system and all RNA integrity number (RIN) were all above 9.5. RNAseq libraries were generated from 500 ng of total RNA using TruSeq Stranded mRNA LT Sample Preparation Kit (Illumina), according to manufacturer's instructions. Briefly, following purification with poly-T oligo attached magnetic beads, the mRNA was fragmented using divalent cations at 94°C for 2 minutes. The cleaved RNA fragments were copied into first strand cDNA using reverse transcriptase and random primers. Strand specificity was achieved by replacing dTTP with dUTP during second strand cDNA synthesis using DNA Polymerase I and RNase H. Following addition of a single 'A' base and subsequent ligation of the adapter on double stranded cDNA fragments, the products were purified and enriched with PCR (30 s at 98°C; [10 s at 98°C, 30 s at 60°C, 30 s at 72°C] x 12 cycles; 5 min at 72°C) to create the cDNA library. Surplus PCR primers were further removed by purification using AMPure XP beads (Beckman-Coulter) and the final cDNA libraries were checked for quality and quantified using capillary electrophoresis. Libraries were sequenced on Hiseq 4000 sequencer (Illumina) as single-end 50 base reads following Illumina's instructions (IGBMC, Genomeast platform), with 3 biological replicates sequenced per condition. We obtained approximately 40 million reads per samples with a minimum of 85% uniquely mapped read per sample. Reads were mapped onto the mm10 assembly of Mus musculus genome (UCSC Genome Browser) using STAR (v2.5.3a). Quantification of gene expression was performed using HTSeq-0.6.1p1, using union mode, with annotations coming from Ensembl version 95. Read counts have been normalized across samples with the median-of-ratios method proposed by Anders and Huber. Comparisons of groups were performed using the test for differential expression implemented in the Bioconductor package DESeq2 (v1.16.1). P-values were adjusted for multiple testing using the Benjamini and Hochberg method. Clustering analysis and heat

maps between groups were generated using R (Bioconductor). Representation of the Q1 to Q4 gene expression groups were also represented on the R-software. Cross-comparison of RNA-seq data were represented of proportional Venn diagram and performed using eulerr in the R software. Gene ontology (GO) associated with the differential expressed genes were analyzed using the DAVID software. The top 10 biological process, cellular component, molecular function and KEGG pathways with FDR adjusted p-value <0.05 were represented on the graphics. Graphics representing the gene expression for the different genotypes and conditions were performed using GraphPad Prism 8 (GraphPad, CA) and are presented as mean ± standard error of the mean (SEM) and normalized to *Fus*$^{+/+}$ HC. Adjusted p-value<0.1 using FDR were considered significant.

2.8. Nuclear extraction for ChIP-seq

A total of two (ChIP-seq FUS) or of four (ChIP-seq of histone modifications) hippocampi were chopped on ice with a razor blade (n = 2 biological replicates per group) and homogenized in PBS with Protein Inhibitor Coktail (PIC, Roche, cOmplete ref#11836145001). Tissues were mechanically dissociated with pipettes and with the dounce B (loose) and then transferred in microcentrifuge tubes for fixation with 1% PFA at RT for 10 min. Cross-linking was stopped by adding 1.67M of glycine at RT for 5 min. Tissues were centrifuged at 4°C, 3600g for 5 min and then incubate in PBS with PIC at 4°C for 5 min, this step was repeated two times. After centrifugation tissues were incubated in cell lysis buffer (10mM HEPES pH8, 85mM KCL, 0,5% NP-40 in ddH2O) with PIC at 4°C for 7 min. Pellet were collected by centrifugation at 4°C, 5000 rpm for 20 min, resuspend in nuclei extraction buffer (0,1% SDS, 10 mM EDTA pH8, 50 mM Tris in ddH20) with PIC at 4°C for 7 min and nuclei were collected after centrifugation at 4°C, 5000 rpm for 10 min. Nuclei were resuspended in PBS with PIC at 4°C for 5 min and centrifuge one last time at 4°C, 5000 rpm for 5 min to obtain a clean pellet of nuclei. For the ChIP-seq FUS, nuclei pellets were frozen at -80 °C until the day of the experimentation. For ChIP-seq of histone modifications, samples were resuspended in cold PBTB (5% BSA, 0.1% Tween-20 in PBS) for filtration with the CellTrics® 50 µm filters (Sysmex, 04-004-2327) and further used for neuronal nuclei staining.

An additional step of fixation was added for the protocol of ChIP-seq experiment against the FUS protein. After tissue dissociation in the Dounce B (loose), samples were transferred in microcentrifuge tubes for fixation with 1:250 of ChIP Cross-link Gold (Diagenode, C01019027) at RT for 30 min, allowing better fixation of higher order protein interactions. Then samples were centrifuged at 4°C 3600g for 5min and washed two times in PBS with PIC before to continue with the fixation of 1%PFA and the next steps of the protocol above.

2.9. Neuronal staining for ChIP-seq of histone modifications

Nuclei preparation for ChIP-seq of histone modification were further prepared for neuronal staining of hippocampal nuclei. Neuronal nuclei were stained using mouse anti-NeuN, 1:1000 (Millipore, Ref: MAB377, Lot: 2967854) in the PBTB (5% BSA, 0.1% Tween-20 in PBS) with addition of 3% normal horse serum. Nuclei were incubated at 4°C during 30 min. For control of no antibody and 2nd antibodies, a few microliters of resuspended nuclei were not incubated with anti-NeuN. sample were centrifuged at 4°C, 5000 rpm during 5 min and wash in 1 ml PBTB with 3% NHS before centrifugation. Nuclei were incubated with the secondary Alexa 488 donkey anti mouse, 1:1500, (Invitrogen, Ref: A21202, Lot: 1022448) in PBTB with 3% NHS at 4°C during 15 min. Nuclei were centrifuged at 4°c, 5000 rpm for 5 min, then washed in PBST (PBS, 0.5% Tween-20), centrifuged and resuspended in PBS for nuclei sorting.

2.10. Neuronal sorting for ChIP-seq of histone modifications

Neuronal and non-neuronal nuclei were collected using the Fluorescent Activated Nuclei Sorting technic (FANS, Aria Fusion), equipped with a 70 µm nozzle at IGBMC (Strasbourg, France). We collected neuronal nuclei with the 488-nm laser. We were able to collect between 1 and 2 Million neurons following this protocol. Nuclei were collected in 1.5 ml low binding tubes, then were centrifuged at 4°C, 5000 rpm for 5 min to remove supernatant and the pellets were frozen at -80°C until ChIP-seq experiment for histone modification.

2.11.1. Chromatin Immunoprecipitation (ChIP) for ChIP-seq of histone modifications

ChIP experiment were always done in two biological replicates per condition. On ice, between 1 and 1.2 million frozen neuronal nuclei were resuspended in 500-600uL Nuclei lysis buffer (10 mM EDTA, 50mM Tris-HCL pH8.1, 1mM NaBu and 1% SDS for H3K4me3, H4K12ac and H3K27ac or 0,4%SDS for H3K27me3, in ddH2O) with PIC in a 15 ml TPX tube (Diagenode). Nuclei were sonicated using the sonicator (Bioruptor Plus sonication device, Diagenode) with 17 cycle of 30sec ON / 30sec OFF on High Power with breaks to vortex tubes every 5 min. 4uL of supernatants were checked on 1,5% agarose gel to confirm DNA fragmentation of approximately bellow 500bp after sonication and between 500bp and 100bp after a rapid decrosslinking protocol. Sonicated chromatin was centrifuged at 4°C, 14000g for 10 min to get rid of debris. Supernatants were diluted in ChIP Dilution buffer (1.1% Triton X-100, 1.2 mM EDTA, 16.7 mM Tris-Cl, pH 8.1, 167 mM NaCl in ddH2O) to obtain a final concentration of 0,1%SDS. Approximately 40 000 nuclei were saved before IP for total input chromatin and the rest of the sample were split in a minimum of 400 000 nuclei per ChIP. Samples were incubated overnight (O/N) at 4°C with the following primary Ab: rabbit anti-H4K12ac, 9µg/ChIP (Diagenode, Ref: C15410331, Lot: A2439P), rabbit anti-H3K4me3,

4,25µg/ChIP (Diagenode, Ref: C15410003-10, Lot: A1052D), rabbit anti-H3K27ac, 3,1µg/ChIP (Abcam, Ref: ab4729, Lot: GR3216173-1), rabbit anti-H3K27me3, 5µg/ChIP (Diagenode, Ref: C15410195, Lot: A0821D). On the next day samples were incubated with 50µl/ChIP magnetic beads (Diagenode, Dynabeads protein A, Ref: 10002D) at 4°C during 2h. Beads were previously washed three times in ChIP dilution buffer with 0,1% SDS and blocked O/N at 4°C with BSA. ChIP-DNA were then washed 5 min in several buffers, using a magnetic rack: Low salt, High Salt, LiCL and TE buffer. ChIP-DNA was then incubated in 300 µl elution buffer (1% SDS, 0.1 M NaHCO3 in ddH2O) at RT for 5 min and at 65°C for 10 min. Cross-linkings were reversed by addition of 0,2M NaCL, O/N at 65°C. Then DNAs were purified with RNAse (Abcam, Ref: ab52579, Lot: GR314429-2) at 37°C for 30 min, and in Proteinase K buffer (Invitrogen, Ref: 100005393, Lot :1834876) at 45°C for 1h. Finally, DNAs were extracted with the MicroChIP Diapure columns (Diagenode, Ref: C03040001) and quantification of DNA concentrations were calculated using the Qubit. All samples reached the minimum of 2µg required for sequencing.

2.11.2. ChIP-sequencing of FUS

ChIP experiment targeting the FUS protein was performed in two biological replicates per condition similar to ChIP-seq for histone modifications. The nuclei pellets of total tissue were resuspended in 700µL Nuclei lysis buffer containing only 0.2% SDS. Nuclei were sonicated with 15 cycles of 30sec ON / 30sec OFF. We used a primary rabbit antibody anti-FUS 15µg/ChIP (Bethyl, Ref: A300-293A, Lot: A300-293A-5).

2.11.3. Quality control, libraries, sequencing and analyses of ChIP-sequencing

Quality control, libraries and sequencing were performed by the GenomEast platform (IGBMC, Strasbourg). ChIP-seq libraries were prepared from 2-10 ng of double-stranded purified DNA using the MicroPlex Library Preparation kit v2 (C05010014, Diagenode s.a., Seraing, Belgium), according to manufacturer's instructions. DNA was first repaired and yielded molecules with blunt ends. Next, stem-loop adaptors with blocked 5’ ends were ligated to the 5’ end of the genomic DNA (gDNA), leaving a nick at the 3’ end. The adaptors cannot ligate to each other and do not have single-strand tails thus non-specific background is avoided. In the final step, the 3’ ends of the gDNA were extended to complete library synthesis and Illumina compatible indexes were added through a PCR amplification (4+7 cycles). Amplified libraries were purified and size-selected using Agencourt AMPure XP beads (Beckman Coulter) to remove unincorporated primers and other reagents. Prior to analyses, DNA libraries were checked for quality and quantified using a 2100 Bioanalyzer (Agilent). The libraries were loaded in the flowcell at 8 pM concentration, and clusters were

generated using the Cbot. Libraries were sequenced on Illumina Hiseq 4000 sequencer as Single-End of 50 base reads following Illumina's instructions. We obtained approximately 50 million reads (ChIP-seq of histone modifications) and 30 million reads (ChIP-seq of FUS) per samples with 75% to 92% uniquely mapped read per sample. Each sample have a minimum of 95% read positions with a base quality score over 30. Sequenced reads were mapped to the Mus musculus genome assembly mm10 (UCSC Genome Browser) using Bowtie. Data were normalized to 20 Million reads.

Mapped reads aligned along the repeated elements within the mouse genome were removed by using RepeatSoaker tools (Dozmorov *et al.*, 2015) for ChIP-seq on histone modifications. Biological duplicates were performed for all marks. Inputs were used as controls. Peak detection of histone marks was performed using SICER v1.1 (Xu *et al.*, 2014) with the following parameters: window size: 200; FDR< 0,003. Gap size parameters were selected according to the score value estimated by statistical method implemented in SICER: selected values of gap size are 600, 400, 1000 and 1600 for H4K12ac, H3K4me3, H3K27ac and H3K27me3 respectively. Replicates in ChIP-seq experiments for the repressive H3K27me3 histone mark were performed on two different sets of animals, and differential analyses were performed after batch correction of the replicates using the removeBatchEffect function from the limma package (Ritchie *et al.*, 2015). Peak detection for the ChIP-seq against FUS was performed using SICER v1.1 (window size: 200; gap size: 200bp; default parameters) (Zang *et al.*, 2009). Peaks were annotated relative to genomic features using Homer AnnotatePeaks v4.9.167 (ChIP-seq of histone modifications) and v.11.1 (ChIP-seq against FUS) with annotation from Ensembl v87. As reference coordinates, we used RefSeq genes for Mouse mm10 genome. Read coverage of peaks was calculated for each sample using bedtools multicov, from BEDTools (Quinlan and Hall, 2010), and differential enrichment analysis for ChIP-seq of histone modifications were performed using DESeq2 (Love *et al.*, 2014) (default parameters, adjusted p_value < 0.05 and no Fold change (FC) selection). The differential analyses of the ChIP-seq against FUS was performed using SICER, with an FDR threshold of 0,01 *set a posteriori*. An input sample was provided for each biological sample.

2.11.4. Analyses of ChIP-seq

Proportional Venn diagram showing the colocalization of histone marks were represented with R using eulerr. PCA analyses, dendrogram, heatmap, MA-plot, Z-score expression and Volcano plot for ChIP-seq data were created with the R software.

For the ChIP-seq analyses, the genomic distribution of the different ChIP-seq was collected with seqMINER v1.2.168,69 (Ye *et al.*, 2011) by using Refseq genes. Mouse mm10 genome

is used as reference coordinates for the gene body and TSS representation and the total read obtained in each experiment was used as reference coordinates for the peak center representation. Graphics were represented with the R software. The distribution of peaks along genic and intergenic region was performed using homer annotations. The gene ontology associated with the differential enriched peaks were analyzed using the Genomic Regions Enrichment of Annotations Tool (GREAT) software v.4.0.4. The Top 15 biological process pathways with FDR adjusted p_value <0.05 were represented on the graphics. Predicted promotor motif associated with the differentially enriched peaks were analyzed using GREAT v.3.0.0. and results showing FDR adjusted p_value <0.05 were represented on the graphics. Peaks colocalization was identify with bedtools. The different tracks showing peaks distribution on the genome was visualized with PyGenomeTracks a tool from Galaxy France, using as inputs normalized bigwig files. Graphic Representing genes in the Q1 to Q4 gene expression group was performed on R.

Heatmaps were generated using Deeptools (Ramirez *et al.*, 2016) v3.5 using the tool bamCoverage to generate bigwigs files with a step of 10 nt. Bigwig files were normalized using the CPM method and reads were extended to a size of 200nt for single-end data and to fragment length for paired-end data. The mean signal was computed over biological replicates with wiggletools (Zerbino *et al.*, 2014). Then, the tool Deeptools computeMatrix v3.5 was used to generate a count matrix at the positions of interest that are regions differentially bound by FUS. Finally, the tool Deeptools plotProfile v3.5 was used to generate mean profile plots and Deeptools plotHeatmap v3.5 was used to generate heatmaps. Differentially bound regions were extracted based on adjusted p-value <= 0.01 and 4 peaks in 2 in SFI, 1 in mt-Ti and 1 in mt-Nd6 were removed because of non-specific over-enrichments.

For the analyses comparing RNAseq data with random genes lists, these were created with the sample function of R and based on random and repeated selection without replacement of subsets of ensembl v78 reference mouse genes (based on the mm10 genome) based on expressed genes with the proportions of each quartile matching those in considered genes lists from the Q1-Q4 groups.
For the analyses comparing FUS ChIP-seq data with random peaks from the histone mark ChIP-seq data in the different quartiles, genes associated to significant FUS Up peaks (1066 peaks corresponding to 1013 genes) were removed from the quartiles, 1013 promoters were extracted from each quartile and their profile and heatmaps were established for each histone mark (H3K27ac, H3K4me3 and H4K12ac). For intra-condition comparison of gene expression (Z-scores) between FUS-bound genes and random genes, the same number of

randomly selected genes that do not bind FUS was retrieved with the proportions of each quartile in randomly selected genes matching those in FUS associated genes.
Violin plots were generated using R v4.1.1 and the packages ggplot2 v3.3.5 (Wickham H. ggplot2: Elegant Graphics for Data Analysis. Springer-Verlag New York, 2009) and ggpubr R package version v0.4.0 (Kassambara A. ggpubr: 'ggplot2' Based Publication Ready Plots. 2020 https://CRAN.R-project.org/package=ggpubr).

2.12. Dendritic spine analyses

Golgi staining

Mice that had underwent a 4-day training in the MWM were killed 4 days later. Brains were collected from MWM-trained mice and home cage (HC) control mice (n=5 per group and conditions). The Rapid Golgi stain kit (FD Neurotechnologies, Inc.) was used according to the manufacturer's instructions. Brain coronal section of 100 µm thickness of the dorsal hippocampal region were made using a Vibratome (VT1000M; Leica). Images of basal and apical dendrites of the CA1 pyramidal neurons were acquired using a brightfield microscope (Explora Nova, La Rochelle, France) using a 100 times magnification for each genotype and conditions. We obtained 8–10 hippocampal sections per animal.

Quantification and analyses of dendritic spines

Dendritic spines were identified based on their morphological appearance. Spines were classified into four different types: Mushroom spines (protrusion with large neck and big head), stubby (big protrusion with no obvious separation between neck or head), thin (protrusion with long neck and small head) and filopodia (protrusion with long neck and no head). For each animal, 6 neurons per animal were analyzed, counting the total number of each different types of spine shapes on a 20µm long segments. A total of 6 segments per neurons were counting comprising 3 basal segments and 3 apical segments. Thus, a total of 36 sections (basal and apical together) per animal were counting in total. The spine density was presented as the number of spines per 20 µm of dendritic length.

Data are presented as mean ± standard error of the mean (SEM). Values of $p < 0.05$ were considered significant and are noted in the text. Graphics and statistical analyses were performed using GraphPad Prism 8 (GraphPad, CA). Genotypes and conditions were compares using the repeated two-way ANOVA with Šidák correction for multiple comparisons.

3. Results

3.1. Paradoxical increase in nuclear genomic binding of FUS in hippocampus of *Fus*$^{\Delta NLS/+}$ mice

We first characterized FUS expression and localization in the hippocampus of *Fus*$^{\Delta NLS/+}$ mice. FUS was highly expressed in dorsal hippocampal neurons of the CA1 region of both genotypes, as shown by double NeuN/FUS immunostaining (**Figure 1A**), with an overall increased FUS staining in *Fus*$^{\Delta NLS/+}$ CA1 neurons, confirmed by increased total FUS protein levels (p=0.0004) (**Figure 1B,C**). Subcellular fractionation followed by western blotting using an antibody recognizing the N-Ter of FUS (i.e. all forms of FUS) indicated that, as expected, *Fus*$^{\Delta NLS/+}$ hippocampi displayed increased cytoplasmic FUS protein while the same amount was found in the nucleus of both genotypes (**Figure 1D**). However, and contrasting to results previously obtained in spinal cord or cortex (Scekic-Zahirovic *et al.*, 2017; Scekic-Zahirovic *et al.*, 2021), levels of wild type FUS as measured using an antibody targeting the C-terminal part of FUS were decreased in both cytoplasmic and nuclear compartments (**Figure 1D**). Short and long exposure of uncropped gels are presented in **Supplemental Data 1**. Thus, in the hippocampus, while mutant FUS accumulates in the cytoplasm, a significant fraction of it remains capable of entering the nucleus despite the absence of NLS.

To address the possible alterations in FUS nuclear functions that could be elicited by the presence of the mutant protein in the nucleus, we performed chromatin immunoprecipitation followed by deep sequencing (ChIP-seq) of FUS in hippocampal nuclei of *Fus*$^{+/+}$ and *Fus*$^{\Delta NLS/+}$ mice, using an antibody recognizing all forms of FUS. Peak calling using SICER identified 3511 peaks for the union of both *Fus*$^{+/+}$ and *Fus*$^{\Delta NLS/+}$ genomes (**Supplementary Table 1**). We sought to characterize whether the pattern of FUS genomic binding was modified by the *Fus*$^{\Delta NLS}$ mutation by leading differential analyses. Principal component analyses (PCA) indicated a clear genotype difference in FUS binding to the genome (**Figure S1A**), and differential analyses using SICER (adjusted p-value ≤ 0.01) identified 1066 enriched- and 710 depleted- peaks for FUS binding (**Figure 2A**). A mild global enrichment of FUS binding in the *Fus*$^{\Delta NLS/+}$ genome as compared to *Fus*$^{+/+}$ controls was visible upon alignment of the peak center using seq-miner (**Figure 2B**). Strikingly, while no significant GO terms were enriched in binding sites with the 710 decreased FUS genomic sites, the 1066 enriched regions bound to FUS presented significant gene ontology associations. For biological processes, enriched regions were related to genes associated to RNA metabolic processes, transcription and cytoskeleton/microtubule-dependent transport (**Figure 2C**); for cellular components, they were clearly associated to ribosomal and mitochondrial subunits (**Figure S1B**). Surprisingly, predicted promoter motifs revealed predominant binding of FUS

on a single DNA motif family, that associated with the different members of the ETS family, including the ETS Like-1 protein

ELK1 and the ETS family transcription factor GA-binding protein GABP (**Figure 2D**). Peak distribution analyses revealed an enrichment of FUS-bound genomic regions at the TSS of genes (47,6%) (**Figure 2E**), whereas depleted ones were mainly located in the intergenic regions (43,1%) (**Figure S1C**). Promoter motif analyses of these Promoter-TSS FUS-target genes confirmed specific enrichment of ETS family motifs, particularly ELK1, and other members such as GABPA (**Figure S1D**). Gene ontology pathway analyses using Database for Annotation, Visualization and Integrated Discovery (DAVID) led to similar results as that found using Genomic Regions Enrichment of Annotations Tool (GREAT), e.g. RNA processing, ribosomes and mitochondria and vesicle transport (**Figure 2F, Figure S1E**) but with the addition of a highly significant biological process related to chromatin organization, chromosomes and euchromatin, including regulation of histone and DNA modifications (**Figure 2F,G**). Examples of genome browser image of individual peaks at the TSS of FUS-target genes are shown (**Figure 2H**), displaying increased FUS binding (orange versus blue), for mitochondrial ribosomal protein L3 (*Mrpl3*), mitochondrial ribosomal protein L30 (*Mrpl30*), microtubule interacting and trafficking domain containing 1 (*Mitd1*), Hemk Methyltransferase Family Member 1 (*Hemk1*) and DNA methyltransferase 1-associated protein 1 (*Dmap1*) genes. Thus, FUS mutation leads to increased FUS levels in the nucleus in the hippocampus, where it is enriched on the TSS of a set of genes, characterized by the presence of an ETS-binding motif, and associated to several functions including RNA metabolism, transcription, transport, ribosomal/mitochondrial and chromatin organization.

3.2. The *Fus* mutation induces enrichment in active chromatin marks in hippocampal neurons

Since mutant FUS led to altered genomic FUS binding, we then asked whether this could be associated to alterations of the neuronal epigenomic landscape and further impact neuronal functions. To this aim, we performed ChIP-seq on several epigenetic marks, specifically on neuronal nuclei sorted by Fluorescent activated cell sorting (FACS) from hippocampal tissue of HC $Fus^{+/+}$ and $Fus^{\Delta NLS/+}$ mice. In both genotypes, the total number of neuronal sorted nuclei were comparable, suggesting that downstream analyses were not biased by neuronal loss. We focused on H3K4me3, H4K12ac and H3K27ac histone marks, as markers of transcriptionally active chromatin, and H3K27me3 as a marker of inactive transcription. PCA and dendrograms using the Simple Error Ratio Estimate (SERE) score of the different ChIP-seq samples demonstrated a clear genotype effect (**Figure S2A,B**). Indeed, in hippocampal neurons of $Fus^{\Delta NLS/+}$ mice, we observed that numbers of genomic loci were significantly enriched in active histone marks: H3K27ac (367 increased peaks), H3K4me3 (2855

increased peaks), and H4K12ac (4151 increased peaks) (**Figure 3A, Supplementary Table 2**), while very few were depleted (respectively, 0, 29 and 40). ChIP-seq experiment targeting repressive H3K27me3 histone mark showed that 251 peaks were significantly depleted in this histone mark, and only 1 was found enriched (**Figure S3A,B**). Together, these results are indicative of some remodeling of chromatin in hippocampal neurons of *Fus*$^{\Delta NLS/+}$ mice, towards chromatin decompaction. We will refer to genes presenting with increased active histone marks as Histone Mark-Enriched Genes (HMEG). Further analysis demonstrated an increase of active histone mark on HMEGs in *Fus*$^{\Delta NLS/+}$ mice as seen on peak centers (**Figure 3B, upper panel**), as well as at TSS genes (**Figure 3B, lower panel**). Genomic distribution of enriched peaks showed an enrichment in the TSS regions for the three histone marks (**Figure S2C**). Examples showing prominent TSS enrichment for H3K4me3, H4K12ac and H3K27ac are shown for the *Kmt2a* gene, a lysine methyltransferase regulating the methylation of H3K4me3, and on the *Grin2a* gene, the glutamate ionotropic receptor NMDA type subunit 2A (**Figure 3C**). This was specific to active histone marks as H3K27me3 repressive mark showed a global decrease on the genome, including on the TSS of genes, while we noted a slight increase at the TTS (**Figure S3C**). We then analyzed the functional categories of HMEGs using GREAT (**Figure 3D**). Significant enrichment of H3K27ac was associated with dendritic and synaptic-related genes, gene affected by H3K4me3 enrichment were mainly associated with histone modification and post-translational modifications of proteins, while H4K12ac increased peaks were observed on genes associated with mRNA processing and mRNA metabolic and catabolic processes. (**Figure 3D**). Depleted H3K27me3-genes were significantly associated with transcription and RNA metabolic processes (**Figure S3D**). Although GO terms substantially differed between the three active histone marks, there was a high overlap between genes showing H3K4me3 and H4K12ac increase enrichment (1764 common peaks), with GO term associated with chromatin modification and peptidyl acetylation and methylation (**Figure S4A-C**). Among those genes, we strikingly observed many chromatin-modifying enzymes such as methyltransferases (e.g. *Kmt2a, Kmt2c*), demethylases (e.g. *Kdm1b, Kdm2a, Kdm2b, Kdm5b, Kdm6b, Kdm7a*), acetyltransferases (e.g *Kat6b, Kat2b, Ep300, Clock*) and lysine deacetylases (e.g. *Hdac2, Hdac3, Hdac5, Sirt3, Sirt5*), suggesting major impacts on chromatin organization. Further, we found that 205 peaks demonstrated increased enrichment for the three active histone marks on genes associated with neuronal/synaptic functions (e.g. *Bdnf, Grin2a, Grin2b, Grin2d, Ntrk2, Nr4a3, Mapt, Mef2c, Mef2d, Ache, Crebbp*) (**Figure S4C**). Interestingly, we found that **GABP1,** was commonly enriched in H3K4me3 and H4K12ac ChIP-seq data (**Figure S4D**). As it is the main promoter motif, with the other ETS member ELK1, that associated to FUS bound genes (**Figure 2D**), this could emphasize some selectivity through which FUS binding sites could be enriched in histone marks at these genomic regions.

In all, these data suggest that the FUS mutant modifies the epigenetic landscape of genes involved in chromatin remodeling, RNA metabolism, and neuronal/synaptic genes.

3.3. The *Fus* mutation impairs hippocampal learning-induced transcriptome

As we observed some chromatin remodeling in *Fus*$^{\Delta NLS/+}$ mice, we hypothesized next that *de novo* gene transcription required for establishment of long-term memory (Dubue *et al.*, 2015) (Remaud *et al.*, 2014) (Chatterjee *et al.*, 2018) could be altered in these mice, and performed RNA sequencing of the dorsal hippocampus at basal state (Home cage, HC) or after 3 days of spatial training in the Morris water maze (MWM) (Learning conditions) in *Fus*$^{\Delta NLS/+}$ mice and WT littermates. Differential analyses (adjusted p_value <0.1, no FC) revealed a clear effect of spatial learning (Learning versus Home Cage, HC) on the transcriptome in the hippocampus for both genotypes (**Figure 4A**, **Figure S5A,B, Supplementary Table 3**). Importantly alterations in gene expression between *Fus*$^{\Delta NLS/+}$ mice and WT occurred mainly upon learning (**Figure 4A,B, Figure S5C**), as only 6 differentially expressed genes (DEG) between WT and *Fus*$^{\Delta NLS/+}$ mice in HC conditions. The one gene significantly up-regulated in *Fus*$^{\Delta NLS/+}$ compared to *Fus*$^{+/+}$ mice was the *Fus* gene itself, in agreement with its auto-regulation function (Humphrey *et al.*, 2020) (Sanjuan-Ruiz *et al.*, 2021) and the increased FUS protein levels we observed in the hippocampi of these mice (**Figure 1A**). Interestingly, learning led to about the same number of DEG in *Fus*$^{+/+}$ and *Fus*$^{\Delta NLS/+}$ mice (590 vs 573), but they were only partially overlapping, with 50% fewer repressed genes (127 vs 264) and 37% more induced genes (446 vs 326) in *Fus*$^{\Delta NLS/+}$ than in *Fus*$^{+/+}$ mice, showing an overall gene activation in *Fus*$^{\Delta NLS/+}$ mice (**Figure 4B**). Gene ontology (GO) analyses confirmed a different transcriptional response to 3 days of training in *Fus*$^{\Delta NLS/+}$ and *Fus*$^{+/+}$ mice especially in up-regulated genes. *Fus*$^{\Delta NLS/+}$ mice upregulated genes primarily associated with neuronal and synaptic related functions (**Figure 4C**), and the expression (z-score) of the 59 neuron/synapse-related genes was significantly increased in *Fus*$^{\Delta NLS/+}$ compared to *Fus*$^{+/+}$ mice at that time point of spatial training (**Figure 4D left**). Some of these genes are associated with glutamatergic (e.g. *Gria2, Gria3, Grin2a, Grin3a* and *Grm5*) as well as GABAergic- (e.g. *Gabra2* and *Gabrb2*) related functions (**Figure 4E**). Contrastingly, in *Fus*$^{+/+}$ mice, upregulated genes in learning conditions were mainly associated with transcription (e.g. transcription factor activity, negative and positive regulation of transcription, transcription factor binding) (**Figure 4C**), and the 61 transcription-related genes were significantly less expressed (z-score) in Fus$^{\Delta NLS/+}$ versus *Fus*$^{+/+}$ mice after training (**Figure 4D right**). As an example, WT mice significantly upregulated several immediate early genes, as well as several transcription factors (including ETS transcription factors *Ets2, Etv1* and *Etv5*, but also *Junb, Max, Rorb* and *Nfkbia*, an inhibitor of the Nfkb transcription factor), and these genes exhibited a dampened transcriptional induction in *Fus*$^{\Delta NLS/+}$ mice in response to

learning (**Figure 4F**). Downregulated genes were enriched in similar GO terms between *Fus*$^{\Delta NLS/+}$ and *Fus*$^{+/+}$ mice, mainly related to extracellular matrix/region/space terms (**Figure S5D**). Thus, the ΔNLS mutation leads to little change in the basal hippocampal transcriptome, but pronounced alterations when the hippocampal neuronal network is solicited by experience, such as spatial memory training, with a notable increased expression of neuronal/synaptic genes and dampening of the induction of immediate early/transcription-related genes.

3.4. Significant alteration of histone chromatin marks in *Fus*$^{\Delta NLS/+}$ mice occurs on highly expressed genes that show inappropriate increased expression upon learning.

We then wanted to identify the chromatin state affected by the FUS mutation. We clustered all genes from our HC RNA-seq data in four quartiles of expression named Q1 to Q4 (Q1 = not expressed or lowly expressed (0-25%), Q2 = middle low expressed (25-50%), Q3 = middle high expressed (50-75%) and Q4 = highly expressed (75-100%)) (**Figure 5A**). As expected, the level of active histone marks correlated with the level of transcription (**Figure 5B)**. Attributing HMEGs to each of the defined quartiles revealed that 73 to 83% of them were belonging to the Q4 highly expressed group of genes (**Figure 5C**), suggesting that FUS mutant affected the open chromatin. We further checked whether HMEGs were correlated with changes in their expression in the *Fus*$^{\Delta NLS/+}$ mice. Transcription levels of HMEGs was then calculated as z-score and showed significantly increased expression in resting *Fus*$^{\Delta NLS/+}$ mice (HC) as well as in learning conditions (MWM) (**Figure 5D**). Additionally, we found a significant interaction of genotype x condition for H4K12ac and H3K4me3 HMEGs (###p= 3.99E-05 and ##p=0.00103, respectively), suggesting that enrichment of histone marks may be primed in Fus mutant chromatin and could be more susceptible to transcriptional changes upon stimulation. This is reminiscent to what we observed when we compared the number of learning-induced genes belonging to the HMEG list (for each mark) in the *Fus*$^{\Delta NLS/+}$ and the *Fus*$^{+/+}$ mice. Indeed, in *Fus*$^{\Delta NLS/+}$ mice, 8,3% learning-induced genes were present in the H3K27ac enriched genes as compared to 4,8% in the *Fus*$^{+/+}$, 42% in the H3K4me3 enriched genes as compared to 31%, and 47,9% in the H4K12ac enriched genes as compared to 37,5% (**Figure 5E**). The latter comparison was significant (p=8,90E-05) using a hypergeometric test, supporting that enrichment in histone mark in resting mice (here H4K12ac) may prime transcription upon stimulation. This was also emphasized by the fact that when assessing overlapping HMEGs (H3K4me3 & H4K12ac, 1657 genes and H3K27ac & H3K4me3 & H4K12ac, 178 genes), no difference was observed in HC mice but a significant increase in transcription was observed upon learning (MWM) (**Figure S6A-B**). Importantly, as control, we tested the distribution of the genes of interest found for the 3 marks from **Figure 5D** (observed Z-scores) to the expected distribution of Z-scores of

random genes, chosen according to the proportion of genes associated to HMEG peaks in each quartile of expression (**Figure S6C**). Theses analyses show that for each histone mark and in each experimental condition, the observed expression of the genes of interest is always significantly different from that of a random selection. We can thus conclude that the overexpression of genes associated to the increased histone marks in *Fus*$^{\Delta NLS/+}$ compared to *Fus*$^{+/+}$ mice that we observed in home cage and learning conditions (Figure 5D) is specific. Therefore, the FUS mutation promotes an enrichment of active histone marks at neuronal genes, favoring their transcription upon stimulation. This can also be appreciated on the heat maps representing gene expression levels of the different sets of HMEGs uniquely increased in *Fus*$^{\Delta NLS/+}$ mice in the four experimental conditions (**Figure S7A**), of which the genome tracks of ChIP-seq and RNA-seq data of four representative genes (the histone methyltransferase *Kmt2a*, the ubiquitine ligase Neural precursor cell expressed developmentally downregulated gene 4-like, *Nedd4l*, the enzyme Beta-1,4-galactosyltransferase 6, *B4galt6*; the purine rich element binding protein A, *Pura*) are shown (**Figure S7B**).

Thus, the FUS mutation seems to lead to remodeling processes in open chromatin regions (containing highly expressed genes), likely promoting aberrant expression of associated genes in response to stimulus, here, spatial learning training.

3.5. A possible link between FUS mutation-induced chromatin alterations and FUS binding.

Lastly, we wanted to test whether the altered chromatin landscape was occurring in the same genomic regions as those binding FUS. We integrated histone mark peaks with the FUS peaks, either enriched (Up, 1066), unchanged (No Diff, 1736) or depleted (Down, 710) in *Fus*$^{\Delta NLS/+}$ versus *Fus*$^{+/+}$ mice (**Figure 6A**). Heatmaps and graphs clearly demonstrated the overlap between histone mark ChIP-seq and the FUS ChIP-seq both in enriched (up) regions and non-differentially-regulated (No diff.) FUS regions. Interestingly, they also evidenced an enrichment in *Fus*$^{\Delta NLS/+}$ versus *Fus*$^{+/+}$ mice, not only for Up-bound genes, but also for No diff-bound genes, suggesting that the functional interaction between FUS and the histone marks could extend beyond FUS binding loci. Yet, the 710 FUS depleted (down) loci remained unchanged highlighting some specificity (**Figure 6A**). We also checked the enrichment in histone marks on a selection of random promoter taken in the different quartiles of gene expression (n=8249-8250 genes/quartile), of which all genes associated to significant FUS Up peaks (1066, i.e. 1013 genes) were removed. As an equivalent to the FUS enriched peaks (Up), 1013 genes were randomly extracted from each quartile and the mean profile was established at their promoter for the three histone marks (**Figure S8A**). We detected a clear enrichment in histone marks on the random promoters belonging to the Q3 and Q4

quartiles. Thus, our results suggest that the presence of mutant FUS may display a wide chromatin remodeling effect on promoters of active genes. We further checked whether this could impact gene transcription. Crossing these ChIP-seq data with RNA-seq data showed that FUS-enriched genes (Up), as well as genes that were not differentially bound by FUS (No diff.), were significantly up-regulated in *Fus*$^{\Delta NLS/+}$ versus *Fus*$^{+/+}$ mice in both Home Cage and Learning conditions, whereas FUS-depleted genes (Down) were not significantly regulated (**Figure 6B**).

As control, we tested the distribution of observed Z-scores of the FUS-bound genes (with) to the expected distribution of Z-scores of randomly-selected genes among genes that do not bind FUS (without). Random genes were chosen according to the proportion of genes associated to FUS peaks in each quartile of expression (**Figure S8B**). Theses analyses show that in each experimental condition, the observed distribution of expression of the FUS-bound genes is significantly different from that of the genes that do not bind FUS. We can thus conclude that the overexpression of genes associated to significant FUS binding enrichment (with) in *Fus*$^{\Delta NLS/+}$ compared to *Fus*$^{+/+}$ mice, in home cage and learning conditions, as observed in Figure 6B, is specific. Next, we further analyzed the pathways associated with both FUS-bound genes and HMEGs. Among the FUS Up-bound genes, only 21 intersected with the 3 HMEGs (**Figure 6C**), among which 9 were significantly associated with “Ubi conjugaison” (Uniprot, Annotated keywords, FDR: 0,0224), 3 with “Neuron projection membrane” (GO, Cellular Component, FDR: 0,0345) and 3 with “Mapk signaling pathway” (WikiPathways, FDR: 0,0393). Overlapping of FUS-enriched genes with a single mark represented more genes: H3K27ac, 49 genes; H3K4me3, 174 genes and H4K12Ac, 289 genes (**Figure 6C**). Cross-comparisons were also done with FUS No diff -bound genes (**Figure S8C**). In all, we found that more than 30% of FUS-bound genes (352/1013 for FUS Up and 408/1311 for FUS No diff) showed significant enrichment in at least one of the three histone marks, suggesting a co-occurrence between these two events. Interestingly, FUS Up and H3K4me3-H4K12ac overlapping-genes, representing 116 genes (**Figure 6D**), of which clustering performed with Search Tool for Recurring Instances of Neighbouring Genes (STRING) revealed significant association with chromatin organization-related terms (red and blue clusters, **Figure 6D**), including DNA methylation, histone modification, methyltransferase complex (blue cluster). Other clusters associated with FUS functions as RNA metabolism (red cluster) and synaptic terms (green cluster). When crossed with RNA-seq, these genes were not regulated in Home Cage *Fus*$^{\Delta NLS/+}$ versus *Fus*$^{+/+}$ mice, but were significantly over-induced in *Fus*$^{\Delta NLS/+}$ mice subjected to spatial training (**Figure 6E**). Again, the overlap of FUS -target genes separately with H4K12ac or H3K4me3 HMEGs revealed respectively 289 genes and 174 genes, of which chromatin terms were significantly enriched (H3K4me3, green cluster; H4K12ac, yellow cluster) (**Figure S9**). Indeed, some of these

genes were chromatin enzymes, e.g. *Dnmt3a*, *Kdm6b*, *Jarid2*, *Ehmt2*, *Carm1*, *Kat6b* or proteins involved in nucleosome organization and transcription, e.g. *Brd2*, *Hira*, *Bml1*, *Sfmbt1*, or *H3f3a*. Main other significant pathways found in these overlaps were related to mRNA/RNA metabolism, processing or splicing and mitochondrial functions, as found in the FUS-targeted genes (**Figures 2C,F and S1B,D,E**). Lastly some clusters identified synaptic, dendritic, and neuronal genes as well as Learning and memory, as being both FUS-targets and HMEGs (**Figure 6D**, green cluster; **Figure S9,** 174 genes, red cluster), and also especially when crossing the ChIP-FUS with H3K27ac HMEGs (e.g. GO_CC: Dendritic spine (4), FDR: 0,0473, post-synapse (9), FDR: 0,0119; Synapse (11), FDR: 0,0280; out of the 49 HMEGs in common with FUS-enriched genes). Thus, besides the known functions of FUS on RNA-related metabolic processes and mitochondrial functions, integration of our data points to a major role of FUS in regulating chromatin organization - through the transcriptional control of many chromatin-remodeling proteins-, and important neuronal functions such as structural plasticity.

3.6. *Fus* mutation impairs memory precision and dendritic spine plasticity

Given the extent of basal epigenetic alterations and spatial learning induced transcriptional alterations, we then asked whether this translated into defects in hippocampal-dependent learning and memory formation, using the spatial reference memory test in the Morris Water Maze (MWM). We evaluated both recent and remote spatial memory. We used a protocol involving 5 days of acquisition followed by two probe trials at 24h and 30 days (**Figure 7A**). Both wild type ($Fus^{+/+}$) and $Fus^{\Delta NLS/+}$ mice showed diminished distance to reach the platform over the 5 days of acquisition training, suggesting ability of learning in both genotypes. However, $Fus^{\Delta NLS/+}$ mice did not further improve performance after 3 days of training, showing a significant decreased performance at day 5 as compared to $Fus^{+/+}$ mice (interaction Day X Genotype $p<0.0116$, performance at day 5: $p=0.0393$) (**Figure 7B**). Importantly, this phenotype was not due to motor problems in $Fus^{\Delta NLS/+}$ mice as we did not observe differences in distance to reach the platform nor in swim speed across genotypes at this early age (**Figure S10A,B**). In the retention trial, $Fus^{+/+}$ mice spent significantly more time in the target quadrant. $Fus^{\Delta NLS/+}$ mice tended to show decreased performance as compared to wild type mice at 24 hours, and this difference was significant when remote memory was tested, 30 days after the last training session (**Figure 7C**). $Fus^{\Delta NLS/+}$ mice crossed significantly less the annulus region than wild type littermates (**Figure 7D**), and did not distinguish efficiently the target quadrant from the adjacent quadrant (**Figure 7E,F** & **Figure S10C,D**). $Fus^{\Delta NLS/+}$ mice also significantly swam at a longer mean distance of the platform compared to $Fus^{+/+}$ mice (**Figure S10E**). Thus, $Fus^{\Delta NLS/+}$ mice display impaired spatial long-term memory as early as 5 months of age, that manifests in a lack of precision

for both recent and remote memories. Synaptic rearrangement during the first 4 days after a spatial memory task represents a major mechanism in learning and memory. We thus checked whether structural plasticity was affected in the *Fus*$^{\Delta NLS/+}$ mice by using Golgi staining to identify dendritic spines based on their morphology. Filopodia have no head and are considered immature. Stubby spines have a protrusion but no head or neck and are less mature than headed spines (thins and mushrooms) (Harris *et al.*, 1992). Learning processes are thought to stabilize mushroom spines to form new synapses (Restivo *et al.*, 2009: Caroni *et al.*, 2014). We quantified dendritic spine morphology in both apical and basal dendrites of pyramidal neurons of the CA1 region of the dorsal hippocampus. These countings were performed in resting mice (Home Cage) and 4 days after the last training in the MWM (**Figure S11A**). Fus$^{\Delta NLS/+}$ mice demonstrate significantly fewer mushroom spines in basal condition and after learning (Genotype effect, p=0.0194) (**Figure 7G,H)**. In all, mature mushroom spines were amongst the mostly affected type of spines in both basal and apical dendritic segments from CA1 neurons (**Figure S11B**). Thus, *Fus*$^{\Delta NLS/+}$ mice presented with abnormal structural plasticity translating into a global decrease of mature dendritic spine number, detectable in both resting and behaving mice.

4. Discussion

In this study, we show that, in the CNS and in particular in the hippocampus, a structure with key functions in learning and memory processes, the FUS protein has important regulatory functions on the epigenetic regulation of chromatin organization. Using *Fus*$^{\Delta NLS/+}$ mice, we found that in hippocampal neurons, despite the mutation of the NLS as observed in ALS patients FUS mutations, FUS levels unexpectedly increased at its genomic target sites, leading to epigenetic changes associated with an enrichment of several active histone marks. FUS associated with RNA metabolism, transcription and mitochondrial -genes, but also more surprisingly, at many genes related to chromatin enzymes and proteins involved in DNA and histone modifications. We also observed that FUS preferentially bound to genes carrying ETS/ELK1-transcription factors binding sites. Further, these reorganizations in chromatin landscape were associated with an aberrant transcriptional response during memory formation, impaired memory precision and a reduced number of mature dendritic spines. Collectively, these results demonstrate that FUS mutation can impact essential neuronal functions such as learning and memory processes through alteration of epigenetic regulation of chromatin organization and of activity-induced transcriptional response. This could have pathophysiological relevance in FUS-related diseases.

Surprisingly, we detected increased FUS amounts in the nucleus of *Fus*$^{\Delta NLS/+}$ hippocampi, as 1066 peaks presented with a significant enrichment of FUS binding in *Fus*$^{\Delta NLS/+}$ compared to *Fus*$^{+/+}$ hippocampi (ChIP-seq data). The mutant FUS protein thus appears to show different nuclear import properties in hippocampus as compared with other CNS regions. Indeed, mutant FUS accumulates in hippocampal nuclei, despite absence of NLS sequence, but not in frontal cortex (Scekic-Zahirovic *et al.*, 2021) or spinal cord (Scekic-Zahirovic *et al.*, 2017). This suggests the existence of cell-type-specific mechanisms of FUS nuclear import. Accumulation of FUS in the nucleus is consistent with previous work suggesting either nuclear aggregation of FUS in patients' cells (Schwartz *et al.*, 2014) or gain-of-function in nuclear bodies (Tan and Manley, 2010). Our results raise the intriguing possibility that mutant FUS could be imported in the nucleus despite the absence of the canonical PY-NLS. Interestingly, Baade and collaborators (Baade *et al.*, 2021) showed that FUS interacts with several nuclear import receptors, mostly TNPO1, but also TNPO3, as well as several importins and exportins. TNPO3, in particular, efficiently imports FUS in the nucleus and FUS/TNPO3 interaction is unchanged in the absence of the PY-NLS. It is thus possible that a variable repertoire of nuclear import receptors leads to different outcomes on FUS nuclear import as observed here. Our results thus show that the effects of FUS NLS mutations are likely more complex in the nucleus than isolated loss of function, and further studies should aim at dissecting the genomic effects of mutant FUS in a cell-specific manner.

FUS is a protein that is known for decades to bind to DNA (Baechtold et al., 1999), and regulate RNApol II (Schwartz *et al.*, 2012) and RNApol III transcription (Tan and Manley, 2010). Previous studies in cultured cells had shown that FUS binds to active chromatin (Yang *et al.*, 2014) and accumulates at TSS of most expressed genes (Schwartz *et al.*, 2012). Binding of FUS to chromatin requires RNA and FUS oligomerization (Yang *et al.*, 2014). FUS (Reber *et al.*, 2021), as well as FUS oncoproteins (Davis *et al.*, 2021) interact with multiple chromatin remodeling proteins and this interaction requires its ability to phase separate (Zuo *et al.*, 2021, Reber *et al.*, 2021). Since FUS also interacts with, and phase separate, RNApol II (Thompson *et al.*, 2018; Burke *et al.*, 2015, Murthy *et al.*, 2021), it is tempting to speculate that FUS-mediated phase separation at active chromatin sites participates in chromatin opening and transcription regulation (Schwartz *et al.*, 2012). It is also possible that FUS mediated phase separation indirectly mediates chromatin opening through recruitment of bound RNAs, such as enhancer RNAs (eRNAs), long-non coding RNAs or several other classes of noncoding RNA (for review see Mangiavacchi *et al.*, 2023, Han and Li, 2022, Studniarek *et al.*, 2021) that were shown to participate in the formation of transcriptional condensates (Li *et al.*, 2021). Interestingly, in cultured cells, loss of FUS affected mostly alternative splicing and mRNA levels of mitochondrial-associated genes

(Schwartz *et al.*, 2012). In addition, we also identified a strong association of FUS-target genes to RNA, ncRNA, rRNA -related metabolic processes, reminiscent with the fact that FUS is related to various levels of RNA metabolism (Picchiarelli and Dupuis, 2020; Popper *et al.*, 2021). Interestingly, functional enrichment analyses GO_Term Cellular Component and Biological Process analyses using GREAT all converged to a highly significant association of FUS-target genes with mitochondrial ribosome (Mrpl, Mrps)-related proteins, more general mitochondrial proteins and also specific sub-units of mitochondrial complex I enzymes. Some of these genes, specifically those related to Mrp/Mrpl displayed large amounts of bound FUS proteins (e.g. *Mrpl3*, *Mrpl30*; Figure 2H). These proteins are encoded by the nuclear genome, synthetized in the cytoplasm, and transported into the mitochondria to be assembled into mitochondrial ribosomes, playing a role in the mitochondrial respiratory chain. Abnormal expression of Mrpl is associated with mitochondrial metabolic disorder and cellular dysfunctions (Huang *et al.*, 2020). Yet, *Mrpl3* is related to neurodegenerative diseases and memory impairment in a spontaneous mutation mouse model (Cahill *et al.*, 2020). Thus, altered expression of FUS target genes such as *Mrpl* genes could directly lead to altered mitochondrial functions and underlie the hippocampal neuronal dysfunctions observed in $Fus^{\Delta NLS/+}$ mice (e.g. memory process alterations). Interestingly, transcriptomic changes associated to down-regulation of ribosomal protein levels and mitochondrial function were reported in the spinal cord of the FUS Δ14 mice bearing a humanized FUS mutation and showing nuclear depletion of FUS (Devoy *et al.*, 2017), further supporting our ChIP-seq results showing direct FUS regulation of ribosomal and mitochondrial genes. In the literature, abnormal mitochondrial shapes, shortening, fragmentations and damage were observed when expressing human mutant FUS in neuronal cell culture (Deng *et al.*, 2015) (Tradewell *et al.*, 2012), in pre- and postsynaptic neuromuscular junctions of human FUS mice model (Sharma *et al.*, 2016) and in FTLD-FUS brain sample (Deng *et al.*, 2015). In all, aberrant mitochondrial functions could also lead to dysregulations of the TCA cycle, release/production of its metabolites (e.g. citrate/acetyl-coA) and generate oxidative phosphorylation, important mechanisms in the regulation of neuronal processes.

Yet, further to these findings, we originally uncovered that the FUS mutation induced FUS binding on genomic sites associated with chromatin organization and histone/DNA modifications. This was accompanied with the induction of epigenetic modifications in $Fus^{\Delta NLS/+}$ neurons, as we demonstrated an increase of epigenetic marks associated with active gene transcription (H3K27ac, H3K4me3 and H4K12ac), mainly at the TSS of highly expressed genes, suggesting that the FUS mutation induces local decompaction of chromatin. These epigenetic changes were mostly found on highly expressed genes, and in genes relevant to RNA metabolism (H4K12ac), neuronal function (H3K27ac) and epigenetic

regulation (H3K4me3). Strikingly, crossing these results with enriched FUS-bound genes showed a strong association to epigenetic regulators of chromatin organization, including e.g. chromatin enzymes (either DNA or histone modifiers), histone binding proteins, or nucleosome remodelers, especially with H3K4me3 and H4K12ac. Notably these genes contained a large number of genes encoding methylation-related enzymes (e.g. EHMT2, JARID2, KDM6B, DNMT3A, CARM1). In all, these suggest that FUS exerts a control on chromatin organization, and any alteration, such as that seen in our animal model, may induce chromatin disorganization and impair neuronal functions. Our correlation studies also emphasized a control of FUS on neuronal and synaptic pathways. Yet, these epigenetic alterations did not translate in vast changes in the basal transcriptome. However, an abnormal transcriptional response took place upon learning, with an upregulation of neuronal and synaptic genes in *Fus*$^{\Delta NLS/+}$ hippocampi while this was not the case in *Fus*$^{+/+}$ ones. The formation and consolidation of long-term memories relies on the coordinated gene expression and synthesis of synaptic proteins (Alberini and Kandel, 2014). These dynamic processes occur within time under the tight regulation of specific epigenomic changes and chromatin reorganization in the hippocampus (Marco *et al.*, 2020). Our epigenomic (ChIP-seq) data showing an enrichment of active histone marks in the *Fus*$^{\Delta NLS/+}$ neuronal euchromatin suggest that neuronal and synaptic gene transcription could be aberrantly over-expressed at the wrong time when the system is challenged by experience, as these genes were not found induced at that time (i.e. upon 3 days of spatial training in the MWM) in our previous studies in WT mice (Chatterjee *et al.*, 2018), nor in this study in *Fus*$^{+/+}$ mice. Thus, such enrichment at resting state could act as a "priming" for synaptic gene transcription upon learning. Additionally, proper enhancer-promoter interactions necessary for memory formation (Marco *et al.*, 2020) may be altered by this opened chromatin state and impact IEG transcription as observed in *Fus*$^{\Delta NLS/+}$ mice. Ultimately, these dysregulations may be at the origin of memory dysfunctions and may also interfere with proper dendritic spine formation in *Fus*$^{\Delta NLS/+}$ mice.

Lastly, it is not known whether FUS can directly bind the DNA or if it requires interactions with other factors, but we found that FUS-enriched genomic binding sites were strongly and uniquely associated to promoters of genes carrying an ETS transcription factor response element. This suggests a strong functional relationship between FUS and ETS transcription factors, consistent with transcriptional co-activation of ETV5 (aka Erm) by FUS in skeletal muscle (Picchiarelli *et al.*, 2019), as well as with the occurrence of fusions between FET proteins, like FUS, and ETS-transcription factors in multiple cancers (Kedage *et al.*, 2016). Here again, this almost exclusive binding of FUS to ETS/ELK1 target genes is not inconsistent with its transcriptional co-activation function of multiple other transcription factors

(Powers *et al.*, 1998), that could be relying either on inducible or more transient interactions. It is also noteworthy that ELK1 has been largely involved in learning and memory processes, as well as regulation of mitochondrial functions (Besnard *et al.*, 2011). Interestingly, the consensus sequence for ETS transcription factors was also found uniquely enriched at the TSS regions presenting with decreased H3K4me3 in *Kmt2a* cKO mice, in which affected genes were involved in transcriptional regulation, chromatin binding, mRNA processing and protein ubiquitination (Kerimoglu *et al.*, 2017). *Kmt2a* cKO mice also showed spatial learning and memory impairment (Kerimoglu *et al.*, 2017). KMT2A (Mll1) is specifically involved in the tri-methylation of H3K4 around the TSS regions of actively transcribed and/or poised genes (Guenther *et al.*, 2005). It is thus tempting to speculate that H3K4me3 enrichment as found in $Fus^{\Delta NLS/+}$ mice on ELK/ETS regions of FUS genes may be a trigger of the further chromatin dysregulations we describe in $Fus^{\Delta NLS/+}$ hippocampi. Yet, dysregulation of H3K4 methylation by methylating or demethylating enzymes has been associated with cognitive diseases (including intellectual disabilities, autism spectrum disorders) (Collins *et al.*, 2019; Iwase *et al.*, 2016; Scandaglia *et al.*, 2017; Vallianatos *et al.*, 2020) and possibly with neurodegenerative diseases such as Alzheimer's disease (AD) and frontotemporal dementia (FTD) (Christopher *et al.*, 2017), and its role into FUS-related diseases merits further investigations.

5. Conclusions

How could our findings add relevance to FUS-related diseases? FUS aggregation and mislocalization is observed in multiple neurological diseases. First, *FUS* germline mutations cause *FUS*-ALS (Kwiatkowski *et al.*, 2009; Vance *et al.*, 2009), and *FUS*-ALS patients show heterozygous mutations of the *FUS* gene, similar to $Fus^{\Delta NLS/+}$ mice. To our knowledge, there is no study investigating memory processes in these patients. Our results argue that beyond motor neuron degeneration, more subtle neurological dysfunction could also be present. Interestingly, *FUS* mutations, have also been observed in rare cases of other neurological diseases such as dementia (including FTD) (Huey *et al.*, 2012; Van Langenhove *et al.*, 2010), chorea (Flies and Veldink, 2020), psychosis (Yan *et al.*, 2010) and essential tremor (Merner *et al.*, 2012). FUS aggregates or FUS mislocalization have been observed in sporadic ALS (Tyzack *et al.*, 2019), sporadic FTD (FTD-FUS) (Snowden *et al.*, 2011), spinocerebellar ataxia (Doi *et al.*, 2010) and Huntington's disease (Kino *et al.*, 2016; Mori *et al.*, 2019). It is thus possible that altered FUS function commonly underlies a number of behavioral defects in neurodegenerative diseases. Further studies should aim at characterizing FUS genomic binding sites in these different diseases to evaluate this possibility. In all, our study highlights a strong functional relationship between FUS and

epigenetic modifications in the context of memory, that may help to understand the potential benefits of epi-therapies (e.g. (Paganoni *et al.*, 2020)) and calls for further investigation in the neurological phenotype of FUS-related diseases.

Availability of data and materials

Datasets generated in the study are deposited in the Gene Expression Omnibus repository at NCBI under accession numbers GSE218226 (RNAseq), GSE218863 (ChIPseq for H3K27ac, H3K4me3 and H4K12ac), GSE218864 (ChIPseq for H3K27me3), and GSE218865 (ChIPseq for FUS).

CRediT authorship contribution statement

Laura Tzeplaeff: performed most of the experiments (Behavior, ChIP-seq, RNA-seq, Golgi staining and spine counting), analyzed data, prepared data visualization and wrote the original draft. **Jonathan Seguin:** performed bioinformatic analyses, analyzed data, data visualization and data storage. **Salim Megat:** performed bioinformatic analyses. **Brigitte Cosquer:** performed animal perfusions and Golgi staining. **Stéphanie Le Gras:** performed bioinformatic analyses, analyzed data and data visualization. **Damien Plassard:** performed bioinformatic analyses, analyzed data and data visualization. **Stéphane Dieterlé:** performed and analyzed Western Blotting experiments and subcellular fractionations. **Isabel Paiva:** helped to set up FACS sorting of hippocampal nuclei. **Gina Picchiarelli:** helped to set up the FUS ChIP-seq experiment. **Charles Decraene:** performed bioinformatic analyses and data storage. **Rafael Alcala Vida:** helped to set up FACS sorting of hippocampal nuclei. **Jean-Christophe Cassel**: reviewed and edited the manuscript. **Karine Merienne :** analyzed data, reviewed and edited the manuscript. **Luc Dupuis :** conceived and supervised the study, analyzed data, secured funding and wrote the original draft. **Anne-Laurence Boutillier :** conceived and supervised the study, analyzed data, secured funding and wrote the original draft. All authors have approved the contents of this manuscript and provided consent for publication.

Competing interests

The authors declare no competing of interests.

Acknowledgements

The authors are grateful to O Bildstein, O Egesi, G Edomwonyi, C Strittmatter and A Isik (UMR 7364), and C De tapia (U1118) for their assistance in animal care. Sequencing was performed by the GenomEast Platform, a member of the 'France Génomique consortium (ANR-10-INBS-0009). We would like to thank Claudine Ebel and Muriel Philipps for their

support in nuclei sorting at the Cytometry Platform (IGBMC, Strasbourg). We thank the Imaging Platform of the CRBS (PIC-STRA UMS 38, Inserm, Unistra) and the Plateforme Imagerie In Vitro de Strasbourg for their help in performing imaging for this study.

Funding

LT was supported by the ANR (EPIFUS, ANR-16-CE92-0031 to ALB and LD) and the Fondation pour la recherche médicale (FDT202001011002 to LT). This work was supported by the CNRS, the University of Strasbourg, ANR (ANR-16-CE92-0031 to ALB and LD, ANR-19-CE17-0016 to LD, ANR-20-CE17-0008 to LD), Fondation pour la Recherche sur le Cerveau (FRC) and Fond de Dotation AFER (2020, ALB), Fondation pour la recherche médicale DEQ20180339179 (LD) and post-doctoral position (SaM), Motor neuron disease association MNDA Dupuis/Apr16/852-791 (LD), Association Française contre les Myopathies (AFM-Téléthon) #23646 (LD), ARSLA (2021 call, LD), Fondation Bettencourt Schueller “Prix Coup d'élan 2019” (LD) and Radala Foundation for ALS Research 2020 (LD).

References

Alberini, C.M., Kandel, E.R., 2014. The regulation of transcription in memory consolidation. *Cold Spring Harb Perspect Biol* 7, a021741.

Armstrong, R.A., Gearing, M., Bigio, E.H., Cruz-Sanchez, F.F., Duyckaerts, C., Mackenzie, I.R., Perry, R.H., Skullerud, K., Yokoo, H., Cairns, N.J., 2011a. Spatial patterns of FUS-immunoreactive neuronal cytoplasmic inclusions (NCI) in neuronal intermediate filament inclusion disease (NIFID). *J Neural Transm (Vienna)* 118, 1651-1657.

Armstrong, R.A., Gearing, M., Bigio, E.H., Cruz-Sanchez, F.F., Duyckaerts, C., Mackenzie, I.R., Perry, R.H., Skullerud, K., Yokoo, H., Cairns, N.J., 2011b. The spectrum and severity of FUS-immunoreactive inclusions in the frontal and temporal lobes of ten cases of neuronal intermediate filament inclusion disease. *Acta Neuropathol* 121, 219-228.

Baade, I., Hutten, S., Sternburg, E.L., Porschke, M., Hofweber, M., Dormann, D., Kehlenbach, R.H., 2021. The RNA-binding protein FUS is chaperoned and imported into the nucleus by a network of import receptors. *J Biol Chem*, 100659.

Baborie, A., Griffiths, T.D., Jaros, E., McKeith, I.G., Burn, D.J., Richardson, A., Ferrari, R., Moreno, J., Momeni, P., Duplessis, D., Pal, P., Rollinson, S., Pickering-Brown, S., Thompson, J.C., Neary, D., Snowden, J.S., Perry, R., Mann, D.M., 2011. Pathological correlates of frontotemporal lobar degeneration in the elderly. *Acta Neuropathol* 121, 365-371.

Baechtold, H., Kuroda, M., Sok, J., Ron, D., Lopez, B.S., Akhmedov, A.T., 1999. Human 75-kDa DNA-pairing protein is identical to the pro-oncoprotein TLS/FUS and is able to promote D-loop formation. *J Biol Chem* 274, 34337-34342.

Baumer, D., Hilton, D., Paine, S.M., Turner, M.R., Lowe, J., Talbot, K., Ansorge, O., Juvenile ALS with basophilic inclusions is a FUS proteinopathy with FUS mutations. *Neurology* 75, 611-618.

Besnard, A., Galan-Rodriguez, B., Vanhoutte, P., Caboche, J., 2011. Elk-1 a transcription factor with multiple facets in the brain. *Front Neurosci* 5, 35.

Burke, K.A., Janke A.M., Rhine C.L., Fawzi N.L. 2015. Residue-by-Residue View of In Vitro FUS Granules that Bind the C-Terminal Domain of RNA Polymerase II. *Mol Cell* 60, 231-241.

Cahill, L.S., Cameron, J.M., Winterburn, J., Macos, P., Hoggarth, J., Dzamba, M., Brudno, M., Nutter, L.M.J., Sproule, T.J., Burgess, R.W., Henkelman, R.M., Sled, J.G., 2020. Structural Variant in Mitochondrial-Associated Gene (MRPL3) Induces Adult-Onset Neurodegeneration with Memory Impairment in the Mouse. *J Neurosci* 40, 4576-4585.

Campbell, R.R., Wood, M.A., 2019. How the epigenome integrates information and reshapes the synapse. *Nat Rev Neurosci* 20, 133-147.

Caroni, P., Chowdhury, A., Lahr, M., 2014. Synapse rearrangements upon learning: from divergent-sparse connectivity to dedicated sub-circuits. *Trends Neurosci* 37, 604-614.

Chatterjee, S., Cassel, R., Schneider-Anthony, A., Merienne, K., Cosquer, B., Tzeplaeff, L., Halder Sinha, S., Kumar, M., Chaturbedy, P., Eswaramoorthy, M., Le Gras, S., Keime, C., Bousiges, O., Dutar, P., Petsophonsakul, P., Rampon, C., Cassel, J.C., Buee, L., Blum, D., Kundu, T.K., Boutillier, A.L., 2018. Reinstating plasticity and memory in a tauopathy mouse model with an acetyltransferase activator. *EMBO Mol Med* 10.

Christopher, M.A., Myrick, D.A., Barwick, B.G., Engstrom, A.K., Porter-Stransky, K.A., Boss, J.M., Weinshenker, D., Levey, A.I., Katz, D.J., 2017. LSD1 protects against hippocampal and cortical neurodegeneration. *Nat Commun* 8, 805.

Cobos, S.N., Bennett, S.A., Torrente, M.P., 2019. The impact of histone post-translational modifications in neurodegenerative diseases. *Biochim Biophys Acta Mol Basis Dis* 1865, 1982-1991.

Collins, B.E., Greer, C.B., Coleman, B.C., Sweatt, J.D., 2019. Histone H3 lysine K4 methylation and its role in learning and memory. *Epigenetics Chromatin* 12, 7.

Davis R.B., Kaur T., Moosa M.M., Banerjee P.R. 2021. FUS oncofusion protein condensates recruit mSWI/SNF chromatin remodeler via heterotypic interactions between prion-like domains. *Protein Sci* 30, 1454-1466.

Deng, J., Yang, M., Chen, Y., Chen, X., Liu, J., Sun, S., Cheng, H., Li, Y., Bigio, E.H., Mesulam, M., Xu, Q., Du, S., Fushimi, K., Zhu, L., Wu, J.Y., 2015. FUS Interacts with HSP60 to Promote Mitochondrial Damage. *PLoS Genet* 11, e1005357.

Devoy, A., Kalmar, B., Stewart, M., Park, H., Burke, B., Noy, S.J., Redhead, Y., Humphrey, J., Lo, K., Jaeger, J., Mejia Maza, A., Sivakumar, P., Bertolin, C., Soraru, G., Plagnol, V., Greensmith, L., Acevedo Arozena, A., Isaacs, A.M., Davies, B., Fratta, P., Fisher, E.M.C., 2017. Humanized mutant FUS drives progressive motor neuron degeneration without aggregation in 'FUSDelta14' knockin mice. *Brain* 140, 2797-2805.

Doi, H., Koyano, S., Suzuki, Y., Nukina, N., Kuroiwa, Y., 2010. The RNA-binding protein FUS/TLS is a common aggregate-interacting protein in polyglutamine diseases. *Neurosci Res* 66, 131-133.

Dozmorov, M.G., Adrianto, I., Giles, C.B., Glass, E., Glenn, S.B., Montgomery, C., Sivils, K.L., Olson, L.E., Iwayama, T., Freeman, W.M., Lessard, C.J., Wren, J.D., 2015. Detrimental effects of duplicate reads and low complexity regions on RNA- and ChIP-seq data. *BMC Bioinformatics* 16 Suppl 13, S10.

Dubue, J.D., McKinney, T.L., Treit, D., Dickson, C.T., 2015. Intrahippocampal Anisomycin Impairs Spatial Performance on the Morris Water Maze. *J Neurosci* 35, 11118-11124.

Fernandez-Albert, J., Lipinski, M., Lopez-Cascales, M.T., Rowley, M.J., Martin-Gonzalez, A.M., Del Blanco, B., Corces, V.G., Barco, A., 2019. Immediate and deferred epigenomic signatures of in vivo neuronal activation in mouse hippocampus. *Nat Neurosci* 22, 1718-1730.

Flies, C.M., Veldink, J.H., 2020. Chorea is a pleiotropic clinical feature of mutated fused-in-sarcoma in amyotrophic lateral sclerosis. *Amyotroph Lateral Scler Frontotemporal Degener*, 1-3.

Fujii, R., Okabe, S., Urushido, T., Inoue, K., Yoshimura, A., Tachibana, T., Nishikawa, T., Hicks, G.G., Takumi, T., 2005. The RNA binding protein TLS is translocated to dendritic spines by mGluR5 activation and regulates spine morphology. *Current biology : CB* 15, 587-593.

Guenther, M.G., Jenner, R.G., Chevalier, B., Nakamura, T., Croce, C.M., Canaani, E., Young, R.A., 2005. Global and Hox-specific roles for the MLL1 methyltransferase. *Proc Natl Acad Sci U S A* 102, 8603-8608.

Han Z., Li W. 2022. Enhancer RNA: What we know and what we can achieve. *Cell Prolif* 55, e13202.

Harris, K.M., Jensen, F.E., Tsao, B., 1992. Three-dimensional structure of dendritic spines and synapses in rat hippocampus (CA1) at postnatal day 15 and adult ages: implications for the maturation of synaptic physiology and long-term potentiation. *J Neurosci* 12, 2685-2705.

Ho, W.Y., Chang, J.C., Tyan, S.H., Yen, Y.C., Lim, K., Tan, B.S.Y., Ong, J., Tucker-Kellogg, G., Wong, P., Koo, E., Ling, S.C., 2019. FUS-mediated dysregulation of Sema5a, an autism-related gene, in FUS mice with hippocampus-dependent cognitive deficits. *Hum Mol Genet* 28, 3777-3791.

Huang, G., Li, H., Zhang, H., 2020. Abnormal Expression of Mitochondrial Ribosomal Proteins and Their Encoding Genes with Cell Apoptosis and Diseases. *Int J Mol Sci* 21.

Huey, E.D., Ferrari, R., Moreno, J.H., Jensen, C., Morris, C.M., Potocnik, F., Kalaria, R.N., Tierney, M., Wassermann, E.M., Hardy, J., Grafman, J., Momeni, P., 2012. FUS and TDP43 genetic variability in FTD and CBS. *Neurobiol Aging* 33, 1016 e1019-1017.

Humphrey, J., Birsa, N., Milioto, C., McLaughlin, M., Ule, A.M., Robaldo, D., Eberle, A.B., Krauchi, R., Bentham, M., Brown, A.L., Jarvis, S., Bodo, C., Garone, M.G., Devoy, A., Soraru, G., Rosa, A., Bozzoni, I., Fisher, E.M.C., Muhlemann, O., Schiavo, G., Ruepp, M.D., Isaacs, A.M., Plagnol, V., Fratta, P., 2020. FUS ALS-causative

mutations impair FUS autoregulation and splicing factor networks through intron retention. *Nucleic Acids Res* 48, 6889-6905.

Ishigaki, S., Fujioka, Y., Okada, Y., Riku, Y., Udagawa, T., Honda, D., Yokoi, S., Endo, K., Ikenaka, K., Takagi, S., Iguchi, Y., Sahara, N., Takashima, A., Okano, H., Yoshida, M., Warita, H., Aoki, M., Watanabe, H., Okado, H., Katsuno, M., Sobue, G., 2017. Altered Tau Isoform Ratio Caused by Loss of FUS and SFPQ Function Leads to FTLD-like Phenotypes. *Cell Rep* 18, 1118-1131.

Iwase, S., Brookes, E., Agarwal, S., Badeaux, A.I., Ito, H., Vallianatos, C.N., Tomassy, G.S., Kasza, T., Lin, G., Thompson, A., Gu, L., Kwan, K.Y., Chen, C., Sartor, M.A., Egan, B., Xu, J., Shi, Y., 2016. A Mouse Model of X-linked Intellectual Disability Associated with Impaired Removal of Histone Methylation. *Cell Rep* 14, 1000-1009.

Kedage, V., Selvaraj, N., Nicholas, T.R., Budka, J.A., Plotnik, J.P., Jerde, T.J., Hollenhorst, P.C., 2016. An Interaction with Ewing's Sarcoma Breakpoint Protein EWS Defines a Specific Oncogenic Mechanism of ETS Factors Rearranged in Prostate Cancer. *Cell Rep* 17, 1289-1301.

Kerimoglu, C., Sakib, M.S., Jain, G., Benito, E., Burkhardt, S., Capece, V., Kaurani, L., Halder, R., Agis-Balboa, R.C., Stilling, R., Urbanke, H., Kranz, A., Stewart, A.F., Fischer, A., 2017. KMT2A and KMT2B Mediate Memory Function by Affecting Distinct Genomic Regions. *Cell Rep* 20, 538-548.

Kino, Y., Washizu, C., Kurosawa, M., Yamada, M., Doi, H., Takumi, T., Adachi, H., Katsuno, M., Sobue, G., Hicks, G.G., Hattori, N., Shimogori, T., Nukina, N., 2016. FUS/TLS acts as an aggregation-dependent modifier of polyglutamine disease model mice. *Sci Rep* 6, 35236.

Kino, Y., Washizu, C., Kurosawa, M., Yamada, M., Miyazaki, H., Akagi, T., Hashikawa, T., Doi, H., Takumi, T., Hicks, G.G., Hattori, N., Shimogori, T., Nukina, N., 2015. FUS/TLS deficiency causes behavioral and pathological abnormalities distinct from amyotrophic lateral sclerosis. *Acta Neuropathol Commun* 3, 24.

Kwiatkowski, T.J., Jr., Bosco, D.A., Leclerc, A.L., Tamrazian, E., Vanderburg, C.R., Russ, C., Davis, A., Gilchrist, J., Kasarskis, E.J., Munsat, T., Valdmanis, P., Rouleau, G.A., Hosler, B.A., Cortelli, P., de Jong, P.J., Yoshinaga, Y., Haines, J.L., Pericak-Vance, M.A., Yan, J., Ticozzi, N., Siddique, T., McKenna-Yasek, D., Sapp, P.C., Horvitz, H.R., Landers, J.E., Brown, R.H., Jr., 2009. Mutations in the FUS/TLS gene on chromosome 16 cause familial amyotrophic lateral sclerosis. *Science* 323, 1205-1208.

Lagier-Tourenne, C., Polymenidou, M., Cleveland, D.W., 2010. TDP-43 and FUS/TLS: emerging roles in RNA processing and neurodegeneration. *Hum Mol Genet* 19, R46-64.

Lagier-Tourenne, C., Polymenidou, M., Hutt, K.R., Vu, A.Q., Baughn, M., Huelga, S.C., Clutario, K.M., Ling, S.C., Liang, T.Y., Mazur, C., Wancewicz, E., Kim, A.S., Watt, A., Freier, S., Hicks, G.G., Donohue, J.P., Shiue, L., Bennett, C.F., Ravits, J., Cleveland, D.W., Yeo, G.W., 2012. Divergent roles of ALS-linked proteins FUS/TLS and TDP-43 intersect in processing long pre-mRNAs. *Nat Neurosci* 15, 1488-1497.

Lee J.H., Wang R., Xiong F., Krakowiak J., Liao Z., Nguyen P.T., Moroz-Omori E.V., Shao J., Zhu X., Bolt M.J., Wu H., Singh P.K., Bi M., Shi C.J., Jamal N., Li G., Mistry R., Jung S.Y., Tsai K.L., Ferreon J.C., Stossi F., Caflisch A., Liu Z., Mancini M.A., Li W. 2021. Enhancer RNA m6A methylation facilitates transcriptional condensate formation and gene activation. *Mol Cell* 19;81, 3368-3385.

Linden, M., Thomsen, C., Grundevik, P., Jonasson, E., Andersson, D., Runnberg, R., Dolatabadi, S., Vannas, C., Luna Santamariotaa, M., Fagman, H., Stahlberg, A., Aman, P., 2019. FET family fusion oncoproteins target the SWI/SNF chromatin remodeling complex. *EMBO Rep* 20.

Love, M.I., Huber, W., Anders, S., 2014. Moderated estimation of fold change and dispersion for RNA-seq data with DESeq2. *Genome Biol* 15, 550.

Mackenzie, I.R., Munoz, D.G., Kusaka, H., Yokota, O., Ishihara, K., Roeber, S., Kretzschmar, H.A., Cairns, N.J., Neumann, M., 2011. Distinct pathological subtypes of FTLD-FUS. *Acta Neuropathol* 121, 207-218.

Mangiavacchi A., Morelli G., Orlando V. 2023. Behind the scenes: How RNA orchestrates the epigenetic regulation of gene expression. *Front Cell Dev Biol*. 11, 1123975.

Marco, A., Meharena, H.S., Dileep, V., Raju, R.M., Davila-Velderrain, J., Zhang, A.L., Adaikkan, C., Young, J.Z., Gao, F., Kellis, M., Tsai, L.H., 2020. Mapping the epigenomic and transcriptomic interplay during memory formation and recall in the hippocampal engram ensemble. *Nat Neurosci* 23, 1606-1617.

Merner, N.D., Girard, S.L., Catoire, H., Bourassa, C.V., Belzil, V.V., Riviere, J.B., Hince, P., Levert, A., Dionne-Laporte, A., Spiegelman, D., Noreau, A., Diab, S., Szuto, A., Fournier, H., Raelson, J., Belouchi, M., Panisset, M., Cossette, P., Dupre, N., Bernard, G., Chouinard, S., Dion, P.A., Rouleau, G.A., 2012. Exome sequencing identifies FUS mutations as a cause of essential tremor. *American Journal of Human Genetics* 91, 313-319.

Mori, S., Honda, H., Ishii, T., Yoshimura, M., Sasagasako, N., Suzuki, S.O., Taniwaki, T., Iwaki, T., 2019. Expanded polyglutamine impairs normal nuclear distribution of fused in sarcoma and poly (rC)-binding protein 1 in Huntington's disease. *Neuropathology* 39, 358-367.

Murthy A.C., Tang W.S., Jovic N., Janke A.M., Seo D.H., Perdikari T.M., Mittal J., Fawzi N.L. 2021. Molecular interactions contributing to FUS SYGQ LC-RGG phase separation and co-partitioning with RNA polymerase II heptads. *Nat Struct Mol Biol* 28, 923-935.

Paganoni, S., Macklin, E.A., Hendrix, S., Berry, J.D., Elliott, M.A., Maiser, S., Karam, C., Caress, J.B., Owegi, M.A., Quick, A., Wymer, J., Goutman, S.A., Heitzman, D., Heiman-Patterson, T., Jackson, C.E., Quinn, C., Rothstein, J.D., Kasarskis, E.J., Katz, J., Jenkins, L., Ladha, S., Miller, T.M., Scelsa, S.N., Vu, T.H., Fournier, C.N., Glass, J.D., Johnson, K.M., Swenson, A., Goyal, N.A., Pattee, G.L., Andres, P.L., Babu, S., Chase, M., Dagostino, D., Dickson, S.P., Ellison, N., Hall, M., Hendrix, K., Kittle, G., McGovern, M., Ostrow, J., Pothier, L., Randall, R., Shefner, J.M., Sherman, A.V., Tustison, E., Vigneswaran, P., Walker, J., Yu, H., Chan, J., Wittes, J., Cohen, J., Klee, J., Leslie, K., Tanzi, R.E., Gilbert, W., Yeramian, P.D., Schoenfeld, D., Cudkowicz, M.E., 2020. Trial of Sodium Phenylbutyrate-Taurursodiol for Amyotrophic Lateral Sclerosis. *N Engl J Med* 383, 919-930.

Picchiarelli, G., Demestre, M., Zuko, A., Been, M., Higelin, J., Dieterle, S., Goy, M.A., Mallik, M., Sellier, C., Scekic-Zahirovic, J., Zhang, L., Rosenbohm, A., Sijlmans, C., Aly, A., Mersmann, S., Sanjuan-Ruiz, I., Hubers, A., Messaddeq, N., Wagner, M., van Bakel, N., Boutillier, A.L., Ludolph, A., Lagier-Tourenne, C., Boeckers, T.M., Dupuis, L., Storkebaum, E., 2019. FUS-mediated regulation of acetylcholine receptor transcription at neuromuscular junctions is compromised in amyotrophic lateral sclerosis. *Nat Neurosci* 22, 1793-1805.

Picchiarelli, G., Dupuis, L., 2020. Role of RNA Binding Proteins with prion-like domains in muscle and neuromuscular diseases. *Cell Stress* 4, 76-91.

Popper, B., Scheidt, T., Schieweck, R., 2021. RNA-binding protein dysfunction in neurodegeneration. *Essays Biochem* 65, 975-986.

Powers, C.A., Mathur, M., Raaka, B.M., Ron, D., Samuels, H.H., 1998. TLS (translocated-in-liposarcoma) is a high-affinity interactor for steroid, thyroid hormone, and retinoid receptors. *Mol Endocrinol* 12, 4-18.

Quinlan, A.R., Hall, I.M., 2010. BEDTools: a flexible suite of utilities for comparing genomic features. *Bioinformatics* 26, 841-842.

Ramirez, F., Ryan, D.P., Gruning, B., Bhardwaj, V., Kilpert, F., Richter, A.S., Heyne, S., Dundar, F., Manke, T., 2016. deepTools2: a next generation web server for deep-sequencing data analysis. *Nucleic Acids Res* 44, W160-165.

Reber S., Jutzi D., Lindsay H., Devoy A., Mechtersheimer J., Levone B.R., Domanski M., Bentmann E., Dormann D., Mühlemann O., Barabino S.M.L., Ruepp M.D. 2021. The

phase separation-dependent FUS interactome reveals nuclear and cytoplasmic function of liquid-liquid phase separation. *Nucleic Acids Res* 49, 7713-7731.

Remaud, J., Ceccom, J., Carponcy, J., Dugue, L., Menchon, G., Pech, S., Halley, H., Frances, B., Dahan, L., 2014. Anisomycin injection in area CA3 of the hippocampus impairs both short-term and long-term memories of contextual fear. *Learn Mem* 21, 311-315.

Restivo, L., Tafi, E., Ammassari-Teule, M., Marie, H., 2009. Viral-mediated expression of a constitutively active form of CREB in hippocampal neurons increases memory. *Hippocampus* 19, 228-234.

Ritchie, M.E., Phipson, B., Wu, D., Hu, Y., Law, C.W., Shi, W., Smyth, G.K., 2015. limma powers differential expression analyses for RNA-sequencing and microarray studies. *Nucleic Acids Res* 43, e47.

Sanjuan-Ruiz, I., Govea-Perez, N., McAlonis-Downes, M., Dieterle, S., Megat, S., Dirrig-Grosch, S., Picchiarelli, G., Piol, D., Zhu, Q., Myers, B., Lee, C.Z., Cleveland, D.W., Lagier-Tourenne, C., Da Cruz, S., Dupuis, L., 2021. Wild-type FUS corrects ALS-like disease induced by cytoplasmic mutant FUS through autoregulation. *Mol Neurodegener* 16, 61.

Scandaglia, M., Lopez-Atalaya, J.P., Medrano-Fernandez, A., Lopez-Cascales, M.T., Del Blanco, B., Lipinski, M., Benito, E., Olivares, R., Iwase, S., Shi, Y., Barco, A., 2017. Loss of Kdm5c Causes Spurious Transcription and Prevents the Fine-Tuning of Activity-Regulated Enhancers in Neurons. *Cell Rep* 21, 47-59.

Scekic-Zahirovic, J., Oussini, H.E., Mersmann, S., Drenner, K., Wagner, M., Sun, Y., Allmeroth, K., Dieterle, S., Sinniger, J., Dirrig-Grosch, S., Rene, F., Dormann, D., Haass, C., Ludolph, A.C., Lagier-Tourenne, C., Storkebaum, E., Dupuis, L., 2017. Motor neuron intrinsic and extrinsic mechanisms contribute to the pathogenesis of FUS-associated amyotrophic lateral sclerosis. *Acta Neuropathol* 133, 887-906.

Scekic-Zahirovic, J., Sanjuan-Ruiz, I., Kan, V., Megat, S., De Rossi, P., Dieterle, S., Cassel, R., Jamet, M., Kessler, P., Wiesner, D., Tzeplaeff, L., Demais, V., Sahadevan, S., Hembach, K.M., Muller, H.P., Picchiarelli, G., Mishra, N., Antonucci, S., Dirrig-Grosch, S., Kassubek, J., Rasche, V., Ludolph, A., Boutillier, A.L., Roselli, F., Polymenidou, M., Lagier-Tourenne, C., Liebscher, S., Dupuis, L., 2021. Cytoplasmic FUS triggers early behavioral alterations linked to cortical neuronal hyperactivity and inhibitory synaptic defects. *Nat Commun* 12, 3028.

Scekic-Zahirovic, J., Sendscheid, O., El Oussini, H., Jambeau, M., Sun, Y., Mersmann, S., Wagner, M., Dieterle, S., Sinniger, J., Dirrig-Grosch, S., Drenner, K., Birling, M.C., Qiu, J., Zhou, Y., Li, H., Fu, X.D., Rouaux, C., Shelkovnikova, T., Witting, A., Ludolph, A.C., Kiefer, F., Storkebaum, E., Lagier-Tourenne, C., Dupuis, L., 2016. Toxic gain of function from mutant FUS protein is crucial to trigger cell autonomous motor neuron loss. *EMBO J* 35, 1077-1097.

Schwartz, J.C., Ebmeier, C.C., Podell, E.R., Heimiller, J., Taatjes, D.J., Cech, T.R., 2012. FUS binds the CTD of RNA polymerase II and regulates its phosphorylation at Ser2. *Genes and Development* 26, 2690-2695.

Schwartz, J.C., Podell, E.R., Han, S.S., Berry, J.D., Eggan, K.C., Cech, T.R., 2014. FUS is sequestered in nuclear aggregates in ALS patient fibroblasts. *Mol Biol Cell* 25, 2571-2578.

Sharma, A., Lyashchenko, A.K., Lu, L., Nasrabady, S.E., Elmaleh, M., Mendelsohn, M., Nemes, A., Tapia, J.C., Mentis, G.Z., Shneider, N.A., 2016. ALS-associated mutant FUS induces selective motor neuron degeneration through toxic gain of function. *Nat Commun* 7, 10465.

Snowden, J.S., Hu, Q., Rollinson, S., Halliwell, N., Robinson, A., Davidson, Y.S., Momeni, P., Baborie, A., Griffiths, T.D., Jaros, E., Perry, R.H., Richardson, A., Pickering-Brown, S.M., Neary, D., Mann, D.M., 2011. The most common type of FTLD-FUS (aFTLD-U) is associated with a distinct clinical form of frontotemporal dementia but is not related to mutations in the FUS gene. *Acta Neuropathol* 122, 99-110.

Studniarek C., Egloff S., Murphy S. 2021. Noncoding RNAs Set the Stage for RNA Polymerase II Transcription. *Trends Genet* 37, 279-291.

Tan, A.Y., Manley, J.L., 2010. TLS inhibits RNA polymerase III transcription. *Mol Cell Biol* 30, 186-196.

Thompson V.F., Victor R.A., Morera A.A., Moinpour M., Liu M.N., Kisiel C.C., Pickrel K., Springhower C.E., Schwartz J.C. 2018 Transcription-Dependent Formation of Nuclear Granules Containing FUS and RNA Pol II. *Biochemistry* 57, 7021-7032.

Tibshirani, M., Tradewell, M.L., Mattina, K.R., Minotti, S., Yang, W., Zhou, H., Strong, M.J., Hayward, L.J., Durham, H.D., 2014. Cytoplasmic sequestration of FUS/TLS associated with ALS alters histone marks through loss of nuclear protein arginine methyltransferase 1. *Hum Mol Genet*.

Tradewell, M.L., Yu, Z., Tibshirani, M., Boulanger, M.C., Durham, H.D., Richard, S., 2012. Arginine methylation by PRMT1 regulates nuclear-cytoplasmic localization and toxicity of FUS/TLS harbouring ALS-linked mutations. *Hum Mol Genet* 21, 136-149.

Tyzack, G.E., Luisier, R., Taha, D.M., Neeves, J., Modic, M., Mitchell, J.S., Meyer, I., Greensmith, L., Newcombe, J., Ule, J., Luscombe, N.M., Patani, R., 2019. Widespread FUS mislocalization is a molecular hallmark of amyotrophic lateral sclerosis. *Brain* 142, 2572-2580.

Udagawa, T., Fujioka, Y., Tanaka, M., Honda, D., Yokoi, S., Riku, Y., Ibi, D., Nagai, T., Yamada, K., Watanabe, H., Katsuno, M., Inada, T., Ohno, K., Sokabe, M., Okado, H., Ishigaki, S., Sobue, G., 2015. FUS regulates AMPA receptor function and FTLD/ALS-associated behaviour via GluA1 mRNA stabilization. *Nat Commun* 6, 7098.

Urwin, H., Josephs, K.A., Rohrer, J.D., Mackenzie, I.R., Neumann, M., Authier, A., Seelaar, H., Van Swieten, J.C., Brown, J.M., Johannsen, P., Nielsen, J.E., Holm, I.E., Dickson, D.W., Rademakers, R., Graff-Radford, N.R., Parisi, J.E., Petersen, R.C., Hatanpaa, K.J., White, C.L., 3rd, Weiner, M.F., Geser, F., Van Deerlin, V.M., Trojanowski, J.Q., Miller, B.L., Seeley, W.W., van der Zee, J., Kumar-Singh, S., Engelborghs, S., De Deyn, P.P., Van Broeckhoven, C., Bigio, E.H., Deng, H.X., Halliday, G.M., Kril, J.J., Munoz, D.G., Mann, D.M., Pickering-Brown, S.M., Doodeman, V., Adamson, G., Ghazi-Noori, S., Fisher, E.M., Holton, J.L., Revesz, T., Rossor, M.N., Collinge, J., Mead, S., Isaacs, A.M., 2010. FUS pathology defines the majority of tau- and TDP-43-negative frontotemporal lobar degeneration. *Acta Neuropathol* 120, 33-41.

Vallianatos, C.N., Raines, B., Porter, R.S., Bonefas, K.M., Wu, M.C., Garay, P.M., Collette, K.M., Seo, Y.A., Dou, Y., Keegan, C.E., Tronson, N.C., Iwase, S., 2020. Mutually suppressive roles of KMT2A and KDM5C in behaviour, neuronal structure, and histone H3K4 methylation. *Commun Biol* 3, 278.

Van Langenhove, T., van der Zee, J., Sleegers, K., Engelborghs, S., Vandenberghe, R., Gijselinck, I., Van den Broeck, M., Mattheijssens, M., Peeters, K., De Deyn, P.P., Cruts, M., Van Broeckhoven, C., 2010. Genetic contribution of FUS to frontotemporal lobar degeneration. *Neurology* 74, 366-371.

Vance, C., Rogelj, B., Hortobagyi, T., De Vos, K.J., Nishimura, A.L., Sreedharan, J., Hu, X., Smith, B., Ruddy, D., Wright, P., Ganesalingam, J., Williams, K.L., Tripathi, V., Al-Saraj, S., Al-Chalabi, A., Leigh, P.N., Blair, I.P., Nicholson, G., de Belleroche, J., Gallo, J.M., Miller, C.C., Shaw, C.E., 2009. Mutations in FUS, an RNA processing protein, cause familial amyotrophic lateral sclerosis type 6. *Science* 323, 1208-1211.

Wang, W.Y., Pan, L., Su, S.C., Quinn, E.J., Sasaki, M., Jimenez, J.C., Mackenzie, I.R., Huang, E.J., Tsai, L.H., 2013. Interaction of FUS and HDAC1 regulates DNA damage response and repair in neurons. *Nat Neurosci* 16, 1383-1391.

Wang, X., Arai, S., Song, X., Reichart, D., Du, K., Pascual, G., Tempst, P., Rosenfeld, M.G., Glass, C.K., Kurokawa, R., 2008. Induced ncRNAs allosterically modify RNA-binding proteins in cis to inhibit transcription. *Nature* 454, 126-130.

Ward, C.L., Boggio, K.J., Johnson, B.N., Boyd, J.B., Douthwright, S., Shaffer, S.A., Landers, J.E., Glicksman, M.A., Bosco, D.A., 2014. A loss of FUS/TLS function leads to impaired cellular proliferation. *Cell death & disease* 5, e1572.

Xu, S., Grullon, S., Ge, K., Peng, W., 2014. Spatial clustering for identification of ChIP-enriched regions (SICER) to map regions of histone methylation patterns in embryonic stem cells. *Methods Mol Biol* 1150, 97-111.

Yan, J., Deng, H.X., Siddique, N., Fecto, F., Chen, W., Yang, Y., Liu, E., Donkervoort, S., Zheng, J.G., Shi, Y., Ahmeti, K.B., Brooks, B., Engel, W.K., Siddique, T., 2010. Frameshift and novel mutations in FUS in familial amyotrophic lateral sclerosis and ALS/dementia. *Neurology* 75, 807-814.

Yang, L., Gal, J., Chen, J., Zhu, H., 2014. Self-assembled FUS binds active chromatin and regulates gene transcription. *Proc Natl Acad Sci U S A* 111, 17809-17814.

Yap, E.L., Greenberg, M.E., 2018. Activity-Regulated Transcription: Bridging the Gap between Neural Activity and Behavior. *Neuron* 100, 330-348.

Ye, T., Krebs, A.R., Choukrallah, M.A., Keime, C., Plewniak, F., Davidson, I., Tora, L., 2011. seqMINER: an integrated ChIP-seq data interpretation platform. *Nucleic Acids Res* 39, e35.

Zang, C., Schones, D.E., Zeng, C., Cui, K., Zhao, K., Peng, W., 2009. A clustering approach for identification of enriched domains from histone modification ChIP-Seq data. *Bioinformatics* 25, 1952-1958.

Zerbino, D.R., Johnson, N., Juettemann, T., Wilder, S.P., Flicek, P., 2014. WiggleTools: parallel processing of large collections of genome-wide datasets for visualization and statistical analysis. *Bioinformatics* 30, 1008-1009.

Zuo L., Zhang G., Massett M., Cheng J., Guo Z., Wang L., Gao Y., Li R., Huang X., Li P., Qi Z. 2021. Loci-specific phase separation of FET fusion oncoproteins promotes gene transcription. *Nat Commun* 12, 1491.

Figure Legends:

Figure 1. Nuclear increased of FUS expression in the hippocampus of *Fus$^{\Delta NLS/+}$* mice.

A: Hippocampal brain section from 5-month-old *Fus$^{+/+}$* and *Fus$^{\Delta NLS/+}$* mice immunostained for Total FUS (green), NeuN (red) and DAPI (blue) in the CA1 brain region.

B: Scheme of the FUS protein (WT) and its mutated form ΔNLS. The recognition site of the N-ter and C-ter antibodies are indicated. NLS, nuclear localization signal.

C: Protein level analyses showing FUS overexpression in the hippocampus of *Fus$^{\Delta NLS/+}$* mice at the age of 5 months. Actin is used as loading control. Lower panel: quantification of the blots using ImageLab. Data are represented as mean ± SEM (n = 6 per group). Unpaired t-test, ***p<0.0001.

D: Western Blot analyses of the nucleo-cytoplasmic location of total (N-ter) FUS (A and B) and WT (C-ter) FUS (A and C) in both *Fus$^{+/+}$* and *Fus$^{\Delta NLS/+}$* mice at the age of 5 months. HDAC1 and SOD1 are respectively used for nuclear and cytoplasmic protein control. Data are represented as mean ± SEM relative to WT HC nuclear expression (n = 6 per group). *p<0.05 , ***p<0.0001 using the unpaired t-test.

Figure 2. Increased FUS binding at specific sets of genes in the hippocampus.

A Volcano plot of the significant differential FUS peaks. Peak calling was performed using SICER. The red line represents the cut off of significance (Adjusted p-value < 0,01 using FDR with no fold change selection), red dots show all peaks with significant difference in FUS enrichment in *Fus$^{\Delta NLS/+}$* mice compare to *Fus$^{+/+}$*. (n=2 biological replicates using a mix of 2 hippocampi per replicate).

B: FUS binding sites aligned at the peak center of *Fus$^{+/+}$* (blue) and *Fus$^{\Delta NLS/+}$* (orange) using seq-miner show a tendency of increased FUS binding in *Fus$^{\Delta NLS/+}$* mice.

C-D: GREAT analyses of the top 15 biological processes (D) and predicted promotor motifs (D) of FUS-enriched genes in the hippocampus. Dashed line represents Binomial adjusted p-value < 0.05.

E: Proportion of peaks falling into several genomic features in the enriched FUS-bound regions. Distant-promoter regions are regions located -20kb/-1Kb away from the TSS, promoter-TSS refers to regions located -1Kb/+100bp around the TSS and TTS refers to regions located -100bp/+1Kb around the TTS. Note that FUS is preferentially located at Promoter-TSS in the FUS-enriched regions.

F: GO analyses performed with DAVID on the list of FUS-bound genes at the promoter-TSS, assessing Biological Process.

G: STRING graphic performed using the gene list of GO_BP isolated from the annotation “Chromatin organization” showing that genes associated to major epigenetic regulations are FUS-target genes. FDR for each pathway highlighted by a color is given.

H: Genome browser visualization of FUS binding on the TSS of mitochondrial ribosomal protein L3 (*Mrpl3*), mitochondrial ribosomal protein L30 (*Mrpl30*), microtubule interacting and trafficking domain containing 1 (*Mitd1*), Hemk Methyltransferase Family Member 1 (*Hemk1*) and DNA methyltransferase 1-associated protein 1 (*Dmap1*) genes in $Fus^{+/+}$ (blue) and $Fus^{\Delta NLS/+}$ (orange) hippocampi.

Figure 3. FUS mutation is associated to an increase in active histone marks at the TSS of genes related to synapses, chromatin modification and RNA processing in hippocampal neurons.

A : Volcano plots representing the differential analyses of H3K27ac (left), H3K4me3 (middle) and H4K12ac (right) in the hippocampus. Peak calling was performed using SICER with FDR<0,003. The red line represents the cut-off of significance used in the differential analyses (Adjusted p_value < 0,05 using FDR with no Fold change selection), red dots show all peaks with significant differential enrichment of histone marks in $Fus^{\Delta NLS/+}$ compared to $Fus^{+/+}$ Mice. n=2 biological replicates per histone mark obtained from FANS sorted neurons of a mix of 4 hippocampi per replicate.

B: Mean profiles established for peak center (upper panel) and TSS (lower panel) with SeqMiner on the for H3K27ac, H3K4me3 and H4K12ac (from left to right) for the two biological replicates. Mean profiles for $Fus^{+/+}$ in blue and $Fus^{\Delta NLS/+}$ in orange. Data are represented as mean ± SEM in blue ($Fus^{+/+}$) or orange ($Fus^{\Delta NLS/+}$) shadow. TSS= transcription start site, TTS = transcription terminal site.

C: Genome browser visualization of H3K27ac, H3K4me3 and H4K12ac binding on Lysine Methyltransferase 2A (*Kmt2a*) and glutamate ionotropic receptor NMDA type subunit 2A (*Grin2a*) genes in Fus+/+ (blue) and $Fus^{\Delta NLS/+}$ (orange) hippocampi (n=2/genotype).

D: GREAT analyses of the top 15 biological processes of H3K27ac (left), H3K4me3 (middle) and H4K12ac (right) -enriched genes in the hippocampus of $Fus^{\Delta NLS/+}$ compared to $Fus^{+/+}$ mice. Dashed line represents binomial adjusted p-value < 0.05.

Figure 4: Dysregulated expression of transcription- and synaptic-related genes in the hippocampus of $Fus^{\Delta NLS/+}$ mice during spatial memory formation.

A: Heat map representing the expression z-score of all significantly dysregulated genes of the RNA-seq analyses in the dorsal hippocampal region, shown per animal (n=3 per group). Adjusted p_value <0.1 using the FDR value with no fold change selection.

B: Number of significant differentially expressed genes in the dorsal hippocampus between $Fus^{\Delta NLS/+}$ and $Fus^{+/+}$ in the HC condition (bar graph on the top), Learning condition compared to HC condition for both $Fus^{+/+}$ and $Fus^{\Delta NLS/+}$ groups (bar graph on the bottom), adjusted p< 0.1 using the FDR value with a Cut off of 100 reads for gene expression and no

fold change selection. The two quantitative Venn diagrams represent the common or uniquely differentially expressed genes. In green the down regulated genes and in red the upregulated genes. (n=3 per group).

C: DAVID analyses of the Top 10 biological processes, molecular function, cellular component and KEGG pathways associated with the upregulated genes in the dorsal hippocampus of the Learning group compared to the HC groupe for *Fus*$^{+/+}$ (blue) and *Fus*$^{\Delta NLS/+}$ mice (orange), with x-axis representing the -log10(FDR p-value) and the dashline delimiting the FDR p-value of 0,05. (n=3 per group).

D: Violin plots representing Z-score expression of genes included found in (C) in the GO term « transcription » and noted in blue (left) and « neuron/synapses » noted in red, (right) in the Learning condition from the RNA-seq analyses. (n=3 per group). ****p<0,0001 with the non-parametric Mann Whitney rank test.

E: RNA-seq data showing the expression of genes in the dorsal hippocampus related to « Transcription » annotation terms in DAVID. Data are represented as mean ± SEM and normalized to *Fus*$^{+/+}$ HC, (n = 3 per group). *adjusted p<0.1 using FDR.

F: RNA-seq data showing the expression of genes in the dorsal hippocampus related to « Neuron and Synapse » annotation terms in DAVID. Data are represented as mean ± SEM and normalized to *Fus*$^{+/+}$ HC, (n = 3 per group). *adjusted p<0.1 using FDR.

Figure 5: integration of ChIP-seq and RNAseq.

A: Transcriptomic results of *Fus*$^{+/+}$ HC stratified by expression levels into quartiles (Q1 to Q4), Q1 = not expressed or lowly expressed (0-25%, n=8250), Q2 = middle low expressed (25-50%, n=8249), Q3 = middle high expressed (50-75%, n=8249) and Q4 = highly expressed (75-100%, n=8249). Presented data is the mean the 3 biological replicates. Data are normalized count values divided by median of transcript length in Kb. Y-axis is in log10 scale.

B: Mean H3K27ac, H3K4me3 and H4K12ac (from left to right) profiles at TSS relative to gene expression obtained from RNA-seq data. Expressed genes were separated into four groups (Q1 to Q4), Q1 = not expressed or lowly expressed (0-25%), Q2 = middle low expressed (25-50%), Q3 = middle high expressed (50-75%) and Q4 = highly expressed (75-100%). (n=3 per group for RNA-seq & for Chip-seq two replicates per histone mark).

C: Proportion of genes associated to histone mark peaks (up) in each quartile of expression (Q1 to Q4) (n=3 per group for RNA-seq & n=2 per histone mark for Chip-seq). Total number of genes used for the analyses is n= 365 for H3K27ac, n = 2832 for H3K4me3, n= 4084 for H4K12ac.

D: Z-score expression of all significant HMEGs in the hippocampus, comparing *Fus*$^{+/+}$ (blue) and *Fus*$^{\Delta NLS/+}$ (orange) mice in both HC (dark color) and Learning (light color)

conditions. (n=3 per group for RNA-seq). $$$$ p<0,0001 when comparing HC vs Learning, ****p<0,0001 when comparing *Fus*$^{\Delta NLS/+}$ vs *Fus*$^{+/+}$, with the non-parametric Mann Whitney rank test. Interaction of genotype x condition was tested using the linear regression model, taking in account that mice were not the same in learning and HC groups. Slope for *Fus*$^{\Delta NLS/+}$ vs *Fus*$^{+/+}$ comparisons: H3K27ac, p= 0.167681 ns, nonsignificant, H3K4me3, ###p= 3.99E-05, H4K12ac, ##p=0.00103.

E: Venny diagrams cross-comparing the learning-induced genes in both *Fus*$^{+/+}$ (blue) and *Fus*$^{\Delta NLS/+}$ (orange) (RNA-seq data) and the HMEGs. The number of genes belonging to HMEGs is noted, as the percentage it represents. The result of a hypergeometric test comparing the number of genes that were induced in *Fus*$^{\Delta NLS/+}$ mice to that induced in *Fus*$^{+/+}$ mice and belonging to the enriched ChIP-seq data set is indicated in brackets, *** p=8,90E-05 for H4K12ac; ns, nonsignificant.

Figure 6: Correlation of FUS-enriched genes with HMEG reveal a link between FUS and chromatin organization.

A: Graphs and associated heap maps indicating the presence of the 3 histone marks H3K27ac, H3K4me3 and H4K12ac at regions showing enriched- (Up, 1066), non-differentially regulated (No Diff., 1736), but not in depleted (Down, 710) FUS binding after ChIP-seq in the hippocampus of *Fus*$^{+/+}$ and *Fus*$^{\Delta NLS/+}$ mice.

B: Violin plots representing Z-score expression from the RNA-seq analyses in Home Cage and Learning conditions (n=3 per group) of unique genes corresponding to the FUS ChIP-seq peaks exclusively found in the three conditions (Up, 1013; No Diff., 1311 and Down, 637). *p<0,05; **p<0,01 when *Fus*$^{+/+}$ is compared to *Fus*$^{\Delta NLS/+}$; $$$$p<0,0001 when HC is compared to Learning, with the non-parametric Mann Whitney rank test; ns, nonsignificant.

C: Venn Diagrams showing the intersection of the FUS Up -bound genes with the 3 (H3K27ac, H3K4me3 and H4K12ac) HMEGs.

D: Intersection between H4K12ac, H3K4me3 and FUS corresponding to 116 HMEGs have been analyzed using the Kmeans clustering function of STRING using 4 clusters. A typical graphic representation is shown on the left panel. Right: Gene ontology (GO) for Biological process (BP), Cellular Component (CC) and Molecular Function (MF), as well as Annotated Keywords (UniProt) highlight significant associations to chromatin organization, DNA methylation and histone modification -related processes (blue and red clusters), additionally to RNA processes (red cluster) and synaptic transmission (green cluster). FDR are given on the right. The four colors correspond to the 4 clusters established in STRING.

E: Violin plots representing Z-score expression from the RNA-seq analyses in Home Cage and Learning conditions (n=3 per group) of unique genes corresponding to the 116

HMEGs *p<0,05 when *Fus*$^{+/+}$ is compared to *Fus*$^{\Delta NLS/+}$; $$$$p<0,0001 when HC is compared to Learning, with the non-parametric Mann Whitney rank test; ns, nonsignificant.

Figure 7: *Fus*$^{\Delta NLS/+}$ mice display spatial memory deficits and impaired structural plasticity.

A: Experimental design: mice (n=11/genotype) underwent 5 days of training for spatial memory in the Morris water maze (MWM), with a first Probe Test (PT1) for recent memory performed at day5 (24h after day 4) and a second probe test (PT2) for remote memory performed 30 days after the last training of day 5.

B: Acquisition (latency to find the SE platform, seconds) during the 5 days of training. Both genotypes displayed significant acquisition of the platform location (*D1 vs D5 : Fus*$^{+/+}$ p<0.0001, *Fus*$^{\Delta NLS/+}$ p<0.0349), but *Fus*$^{\Delta NLS/+}$ mice (orange) no longer show improvement after 3d training whereas *Fus*$^{+/+}$ mice (blue) did (repeated two-way ANOVA followed by Šidák correction for multiple comparisons, interaction Day x Genotype p=0.0772). *Fus*$^{\Delta NLS/+}$ mice presented a significant decrease in acquisition compared to *Fus*$^{+/+}$ mice at day 5 (repeated two-way ANOVA with Šidák correction for multiple comparisons,* p=0.0393).

C: Retention (Probe tests) at 24h and 30 days. *Fus*$^{\Delta NLS/+}$ mice did not show significant recent memory compared to chance contrary to *Fus*$^{+/+}$ mice (Student's t-test to a constant value, $<0,05), however their time in the target quadrant was not significantly different from them (two-way ANOVA with Šidák correction for multiple comparisons, non-significant, p=0,06). Remote memory was not significantly impaired when compared to chance for both genotypes ($<0.05) but *Fus*$^{\Delta NLS/+}$ mice showed significantly decreased performance in the target quadrant compared to *Fus*$^{+/+}$ mice (*p<0.01) suggesting a lack of precision. $ when compared to chance (dotted line, 15 s). * for genotype comparisons. Bar graphs are mean ± SEM.

D: Annulus crossing was significantly less in *Fus*$^{\Delta NLS/+}$ mice compared to *Fus*$^{+/+}$ mice at both retention times (non-parametric unpaired Man-Whitney rank test, p=0,05 at 24h and *p<0,05 at 30d). Bar graphs are mean ± SEM.

E,F: Mean heatmaps of the probe tests (left) and their quantification (right) showing that *Fus*$^{\Delta NLS/+}$ mice spend equal time in one of the adjacent quadrants and in the target quadrant at both retention times (24h and 30d), while *Fus*$^{+/+}$ mice spend significantly more time in the target quadrant (two-way ANOVA with Šidák correction for multiple comparisons, *p<0.001), confirming the lack of precision of *Fus*$^{\Delta NLS/+}$ mice. Bar graphs are mean ± SEM. T, target quadrant; Adj, adjacent quadrant.

G: Mice received 4 days of training, and mushroom-shaped spines were counted in dorsal CA1, 4 days post-training. Typical examples of a 20µm dendritic fragment bearing

spines after Golgi staining is shown for each condition (n=5 mice/genotype/condition). HC, Home-Cage; MWM, Morris Water Maze.

H: Quantification of mature spines in CA1 dorsal hippocampi presented per 20µm of dendritic segments. The number of mature spines was significantly decreased in *Fus*$^{\Delta NLS/+}$ versus *Fus*$^{+/+}$ mice, whether basal (HC) or after learning (MWM). Repeated two-way ANOVA with Šidák correction for multiple comparisons., Genotype effect, * p=0.0194. A total of 36 dendritic segments per group were counted (6 neurons per animal with each 3 basal and 3 apical segments). Bar graphs are mean ± SEM.

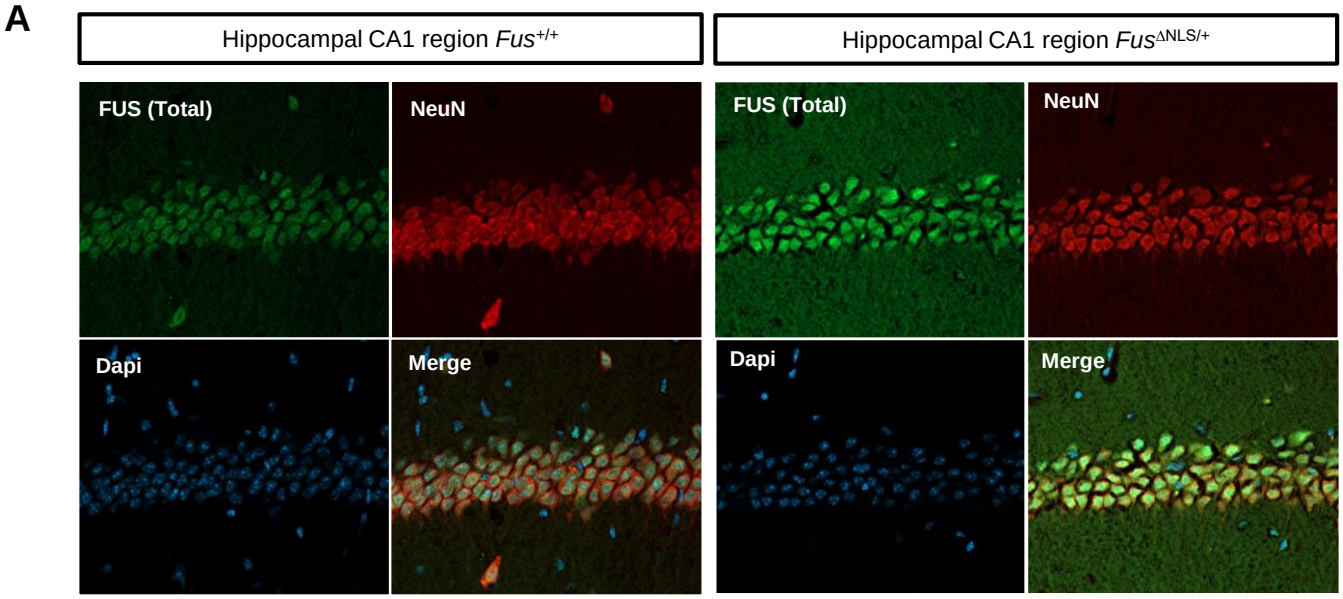
A
Hippocampal CA1 region Fus+/+
Hippocampal CA1 region FusΔNLS/+
FUS (Total)
NeuN
Dapi
Merge
FUS (Total)
NeuN
Dapi
Merge

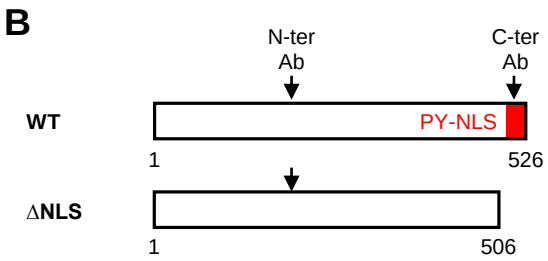
B
N-ter Ab
C-ter Ab
WT
PY-NLS
1
526
ΔNLS
1
506

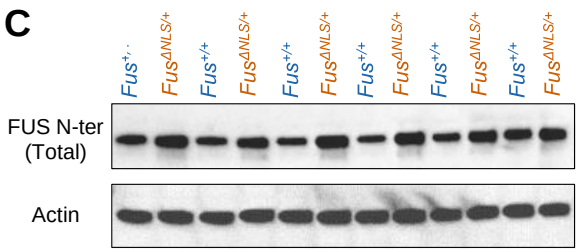
C
Fus+/+
FusΔNLS/+
FUS N-ter (Total)
Actin

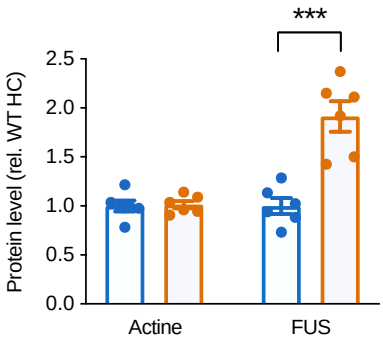
***
Protein level (rel. WT HC)
2.5
2.0
1.5
1.0
0.5
0.0
Actine
FUS

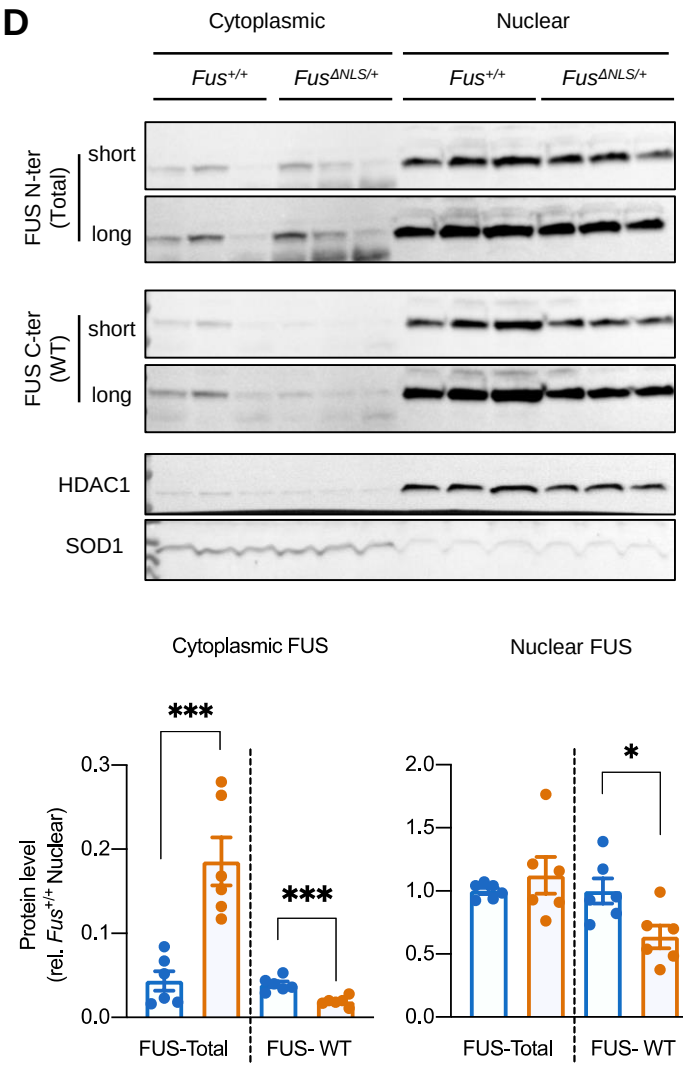
D
Cytoplasmic
Nuclear
Fus+/+
FusΔNLS/+
Fus+/+
FusΔNLS/+
FUS N-ter (Total)
short
long
FUS C-ter (WT)
short
long
HDAC1
SOD1
Cytoplasmic FUS
Nuclear FUS
***
***
*
Protein level (rel. Fus+/+ Nuclear)
0.3
0.2
0.1
0.0
2.0
1.5
1.0
0.5
0.0
FUS-Total
FUS- WT
FUS-Total
FUS- WT

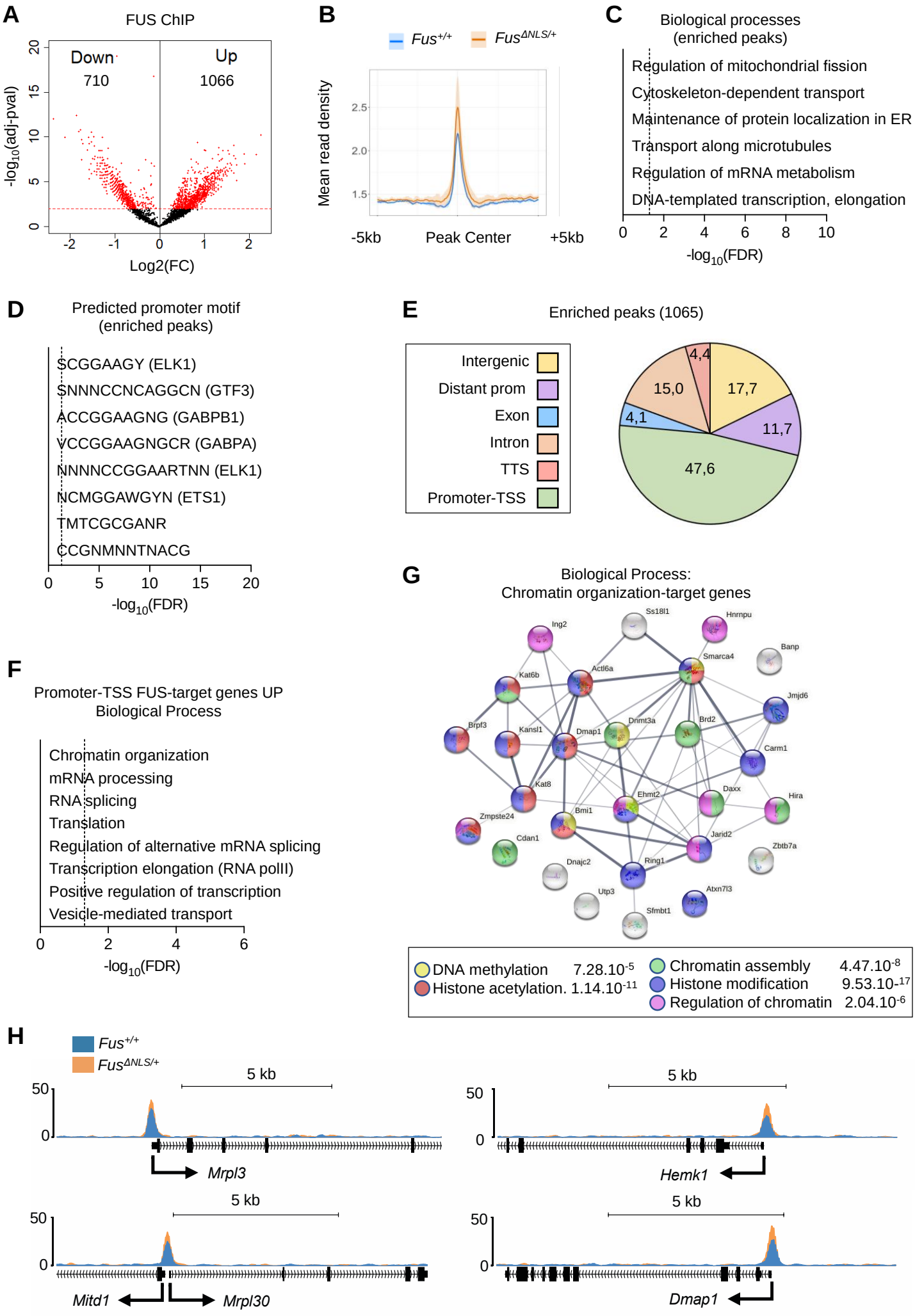
A
FUS ChIP
Down
710
Up
1066
-log10(adj-pval)
Log2(FC)
B
Fus+/+
FusΔNLS/+
Mean read density
-5kb
Peak Center
+5kb
C
Biological processes
(enriched peaks)
Regulation of mitochondrial fission
Cytoskeleton-dependent transport
Maintenance of protein localization in ER
Transport along microtubules
Regulation of mRNA metabolism
DNA-templated transcription, elongation
-log10(FDR)
D
Predicted promoter motif
(enriched peaks)
SCGGAAGY (ELK1)
SNNNCCNCAGGCN (GTF3)
ACCGGAAGNG (GABPB1)
VCCGGAAGNGCR (GABPA)
NNNNCCGGAARTNN (ELK1)
NCMGGAWGYN (ETS1)
TMTCGCGANR
CCGNMNNTNACG
-log10(FDR)
E
Enriched peaks (1065)
Intergenic
Distant prom
Exon
Intron
TTS
Promoter-TSS
4,4
15,0
17,7
4,1
11,7
47,6
F
Promoter-TSS FUS-target genes UP
Biological Process
Chromatin organization
mRNA processing
RNA splicing
Translation
Regulation of alternative mRNA splicing
Transcription elongation (RNA polII)
Positive regulation of transcription
Vesicle-mediated transport
-log10(FDR)
G
Biological Process:
Chromatin organization-target genes
Ing2
Ss18l1
Hnrnpu
Banp
Smarca4
Actl6a
Kat6b
Jmjd6
Brpf3
Kansl1
Dmap1
Dnmt3a
Brd2
Carm1
Kat8
Ehmt2
Daxx
Hira
Zmpste24
Bmi1
Cdan1
Jarid2
Zbtb7a
Dnajc2
Ring1
Utp3
Atxn7l3
Sfmbt1
DNA methylation 7.28.10-5
Histone acetylation. 1.14.10-11
Chromatin assembly 4.47.10-8
Histone modification 9.53.10-17
Regulation of chromatin 2.04.10-6
H
Fus+/+
FusΔNLS/+
5 kb
Mrpl3
Hemk1
Mitd1
Mrpl30
Dmap1

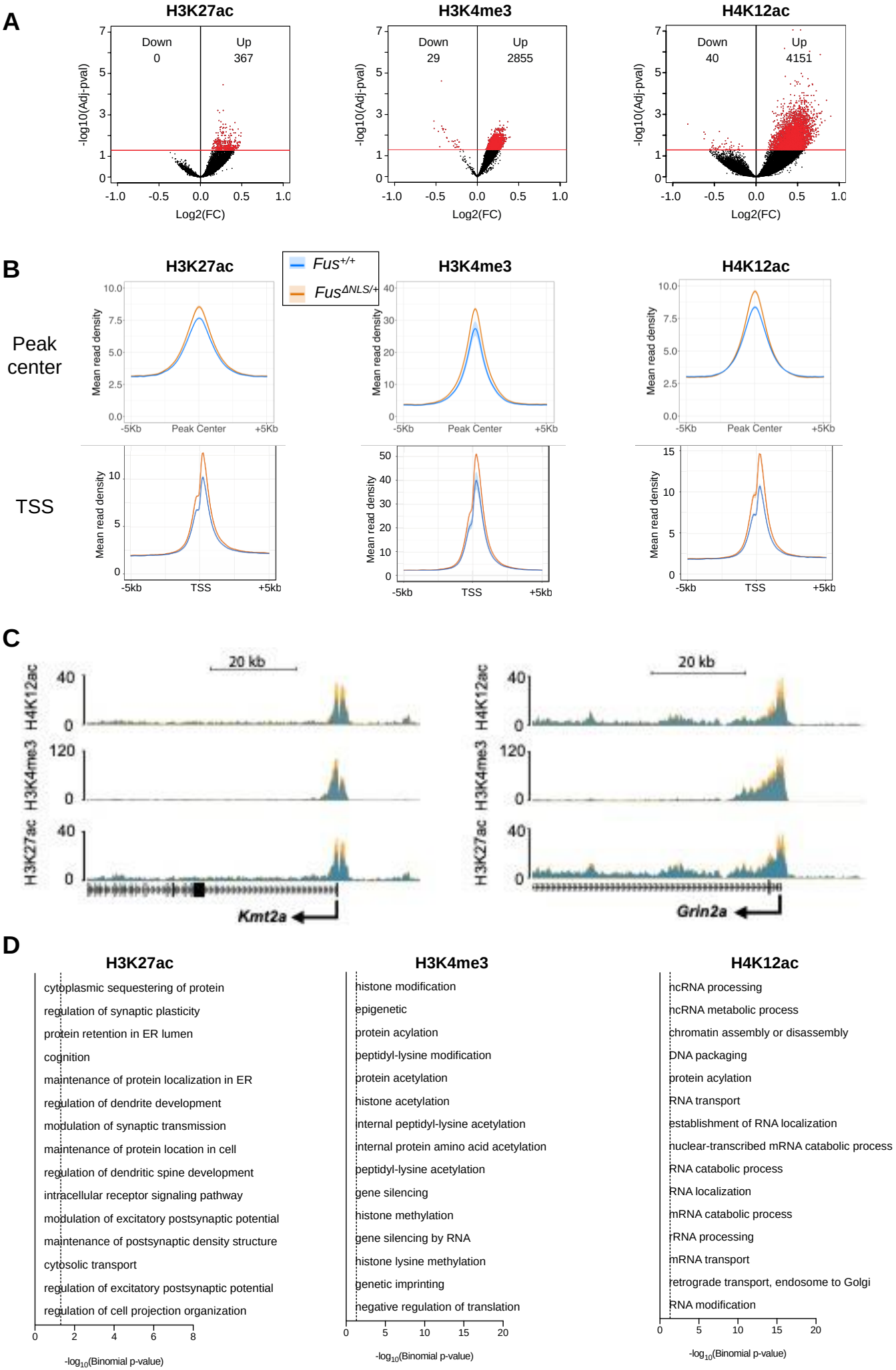
A
H3K27ac
Down
0
Up
367
H3K4me3
Down
29
Up
2855
H4K12ac
Down
40
Up
4151
-log10(Adj-pval)
Log2(FC)
B
Fus+/+
FusΔNLS/+
Peak center
TSS
Mean read density
-5Kb
Peak Center
+5Kb
-5kb
TSS
+5kb
C
20 kb
H4K12ac
H3K4me3
H3K27ac
Kmt2a
Grin2a
D
H3K27ac
cytoplasmic sequestering of protein
regulation of synaptic plasticity
protein retention in ER lumen
cognition
maintenance of protein localization in ER
regulation of dendrite development
modulation of synaptic transmission
maintenance of protein location in cell
regulation of dendritic spine development
intracellular receptor signaling pathway
modulation of excitatory postsynaptic potential
maintenance of postsynaptic density structure
cytosolic transport
regulation of excitatory postsynaptic potential
regulation of cell projection organization
H3K4me3
histone modification
epigenetic
protein acylation
peptidyl-lysine modification
protein acetylation
histone acetylation
internal peptidyl-lysine acetylation
internal protein amino acid acetylation
peptidyl-lysine acetylation
gene silencing
histone methylation
gene silencing by RNA
histone lysine methylation
genetic imprinting
negative regulation of translation
H4K12ac
ncRNA processing
ncRNA metabolic process
chromatin assembly or disassembly
DNA packaging
protein acylation
RNA transport
establishment of RNA localization
nuclear-transcribed mRNA catabolic process
RNA catabolic process
RNA localization
mRNA catabolic process
rRNA processing
mRNA transport
retrograde transport, endosome to Golgi
RNA modification
-log10(Binomial p-value)

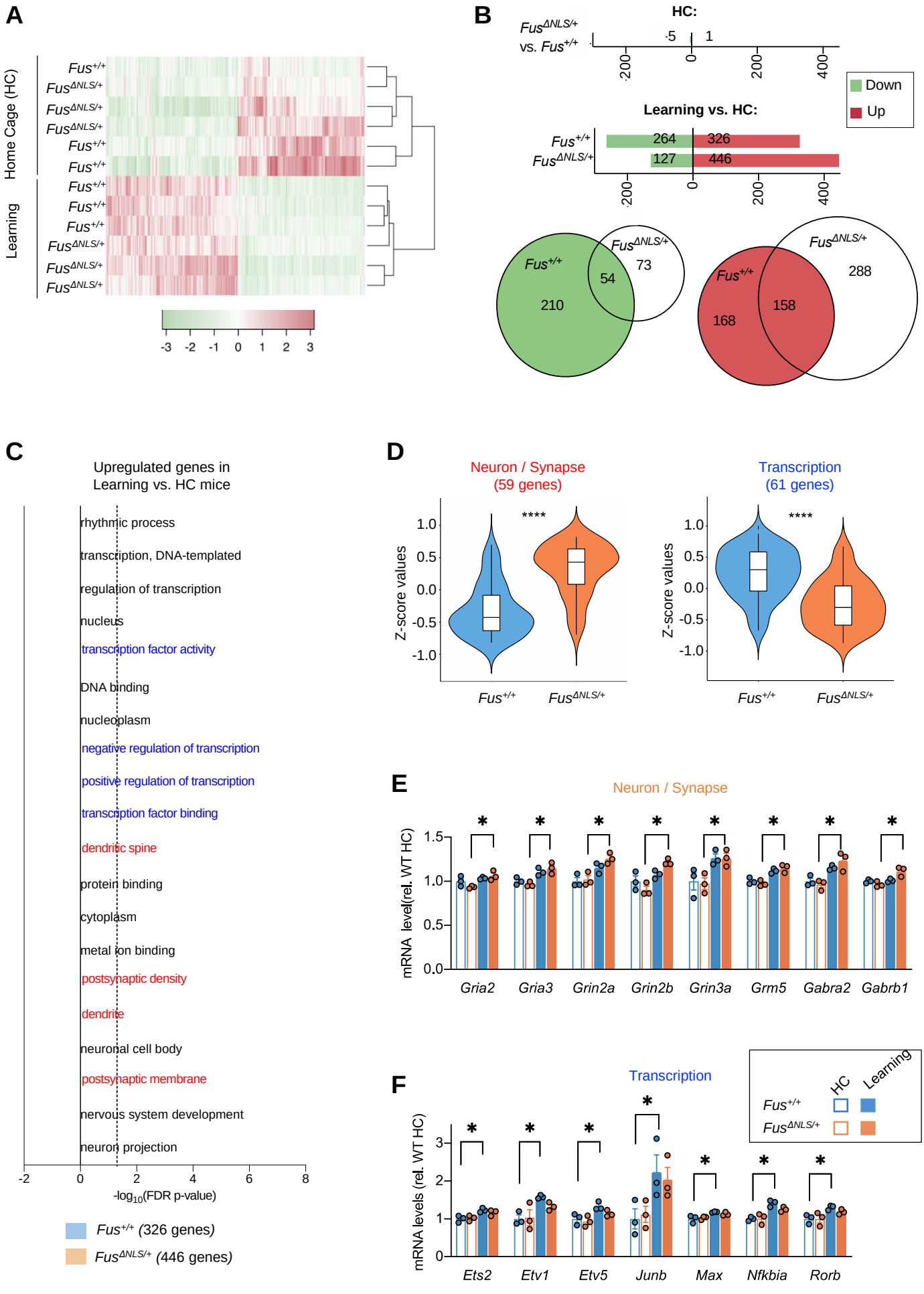
A
Home Cage (HC)
Learning
Fus+/+
FusΔNLS/+
-3 -2 -1 0 1 2 3
B
HC:
FusΔNLS/+ vs. Fus+/+
-5
1
-200
0
200
400
Down
Up
Learning vs. HC:
Fus+/+
FusΔNLS/+
264
326
127
446
Fus+/+
FusΔNLS/+
210
54
73
Fus+/+
FusΔNLS/+
168
158
288
C
Upregulated genes in Learning vs. HC mice
rhythmic process
transcription, DNA-templated
regulation of transcription
nucleus
transcription factor activity
DNA binding
nucleoplasm
negative regulation of transcription
positive regulation of transcription
transcription factor binding
dendritic spine
protein binding
cytoplasm
metal ion binding
postsynaptic density
dendrite
neuronal cell body
postsynaptic membrane
nervous system development
neuron projection
-2 0 2 4 6 8
-log10(FDR p-value)
Fus+/+ (326 genes)
FusΔNLS/+ (446 genes)
D
Neuron / Synapse (59 genes)
Transcription (61 genes)
Z-score values
1.0
0.5
0.0
-0.5
-1.0
****
Fus+/+
FusΔNLS/+
E
Neuron / Synapse
mRNA level(rel. WT HC)
1.5
1.0
0.5
0.0
*
Gria2
Gria3
Grin2a
Grin2b
Grin3a
Grm5
Gabra2
Gabrb1
F
Transcription
mRNA levels (rel. WT HC)
3
2
1
0
HC
Learning
Fus+/+
FusΔNLS/+
Ets2
Etv1
Etv5
Junb
Max
Nfkbia
Rorb

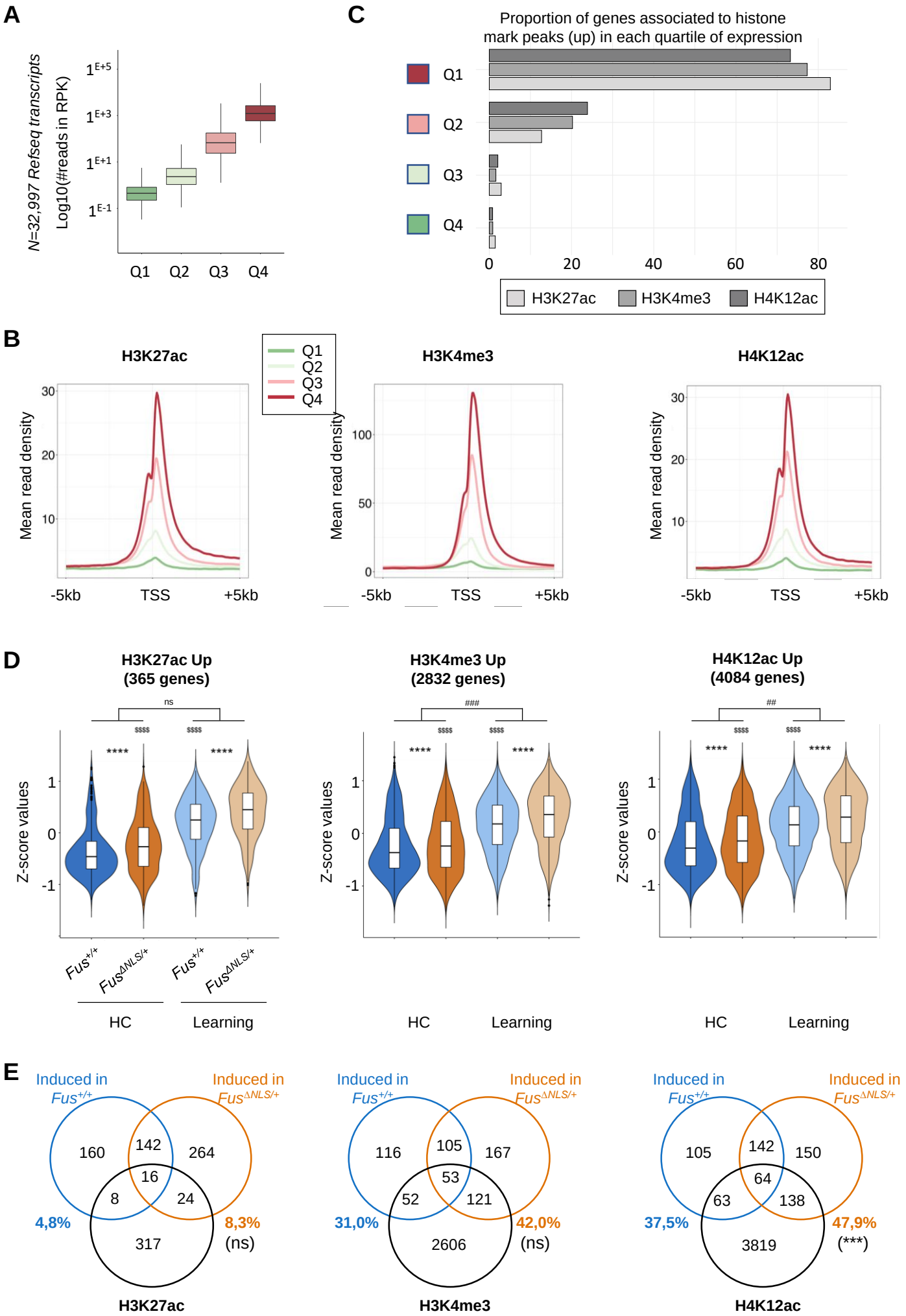
A
N=32,997 Refseq transcripts
Log10(#reads in RPK)
1E+5
1E+3
1E+1
1E-1
Q1
Q2
Q3
Q4
C
Proportion of genes associated to histone mark peaks (up) in each quartile of expression
Q1
Q2
Q3
Q4
0
20
40
60
80
H3K27ac
H3K4me3
H4K12ac
B
H3K27ac
H3K4me3
H4K12ac
Q1
Q2
Q3
Q4
Mean read density
-5kb
TSS
+5kb
D
H3K27ac Up
(365 genes)
H3K4me3 Up
(2832 genes)
H4K12ac Up
(4084 genes)
Z-score values
ns
###
##
****
$$$$
Fus+/+
FusΔNLS/+
HC
Learning
E
Induced in Fus+/+
Induced in FusΔNLS/+
160
142
264
16
8
24
317
4,8%
8,3%
(ns)
H3K27ac
116
105
167
53
52
121
2606
31,0%
42,0%
(ns)
H3K4me3
105
142
150
64
63
138
3819
37,5%
47,9%
(***)
H4K12ac

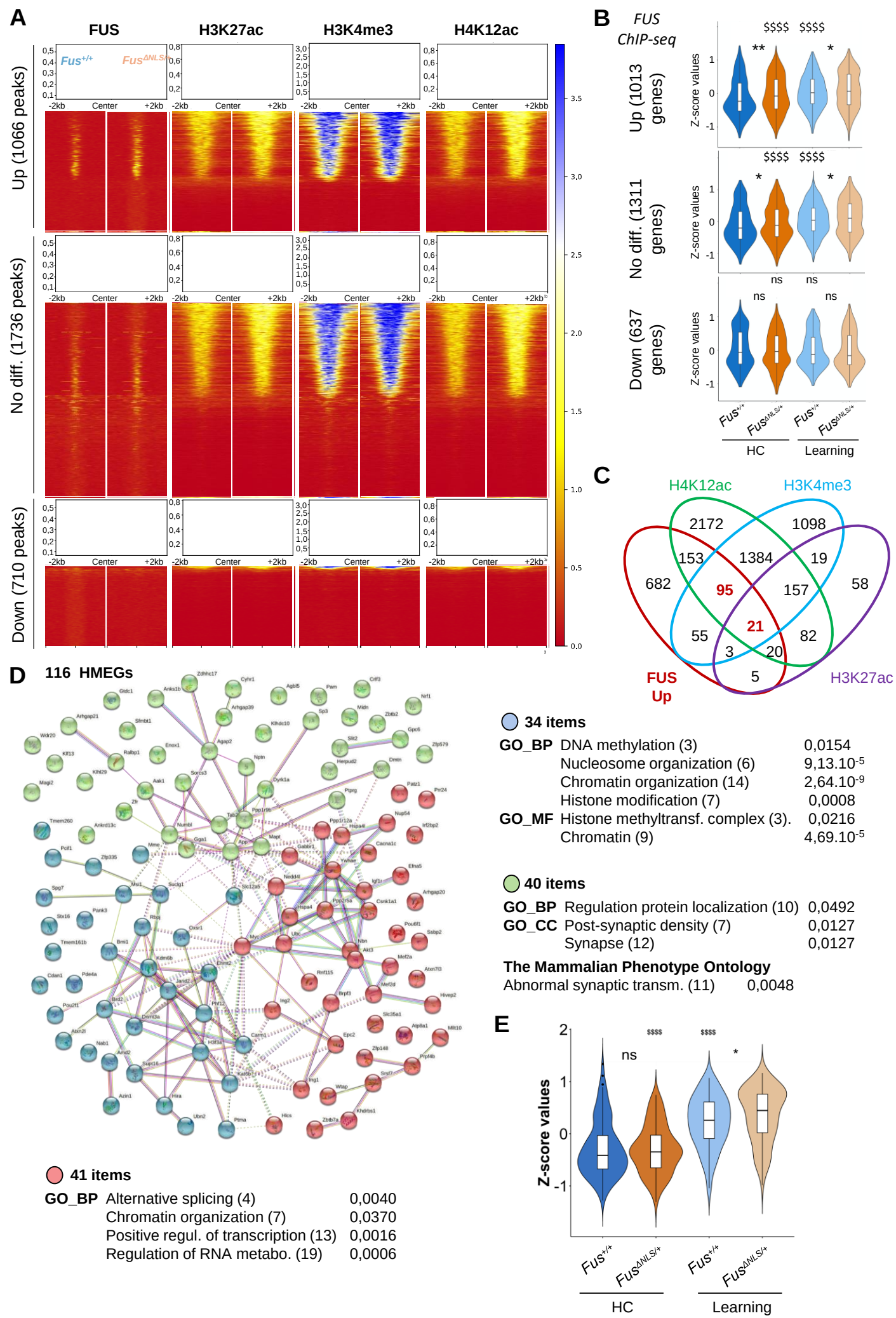
A
FUS
H3K27ac
H3K4me3
H4K12ac
Up (1066 peaks)
No diff. (1736 peaks)
Down (710 peaks)
Fus+/+
FusΔNLS/+
-2kb
Center
+2kb
B
FUS ChIP-seq
Up (1013 genes)
No diff. (1311 genes)
Down (637 genes)
Z-score values
$$$$
**
*
ns
HC
Learning
C
H4K12ac
H3K4me3
H3K27ac
FUS Up
2172
1098
153
1384
19
682
95
157
58
55
21
82
3
20
5
D
116 HMEGs
34 items
GO_BP DNA methylation (3) 0,0154
Nucleosome organization (6) 9,13.10-5
Chromatin organization (14) 2,64.10-9
Histone modification (7) 0,0008
GO_MF Histone methyltransf. complex (3). 0,0216
Chromatin (9) 4,69.10-5
40 items
GO_BP Regulation protein localization (10) 0,0492
GO_CC Post-synaptic density (7) 0,0127
Synapse (12) 0,0127
The Mammalian Phenotype Ontology
Abnormal synaptic transm. (11) 0,0048
41 items
GO_BP Alternative splicing (4) 0,0040
Chromatin organization (7) 0,0370
Positive regul. of transcription (13) 0,0016
Regulation of RNA metabo. (19) 0,0006
E
Z-score values
ns
$$$$
*
HC
Learning

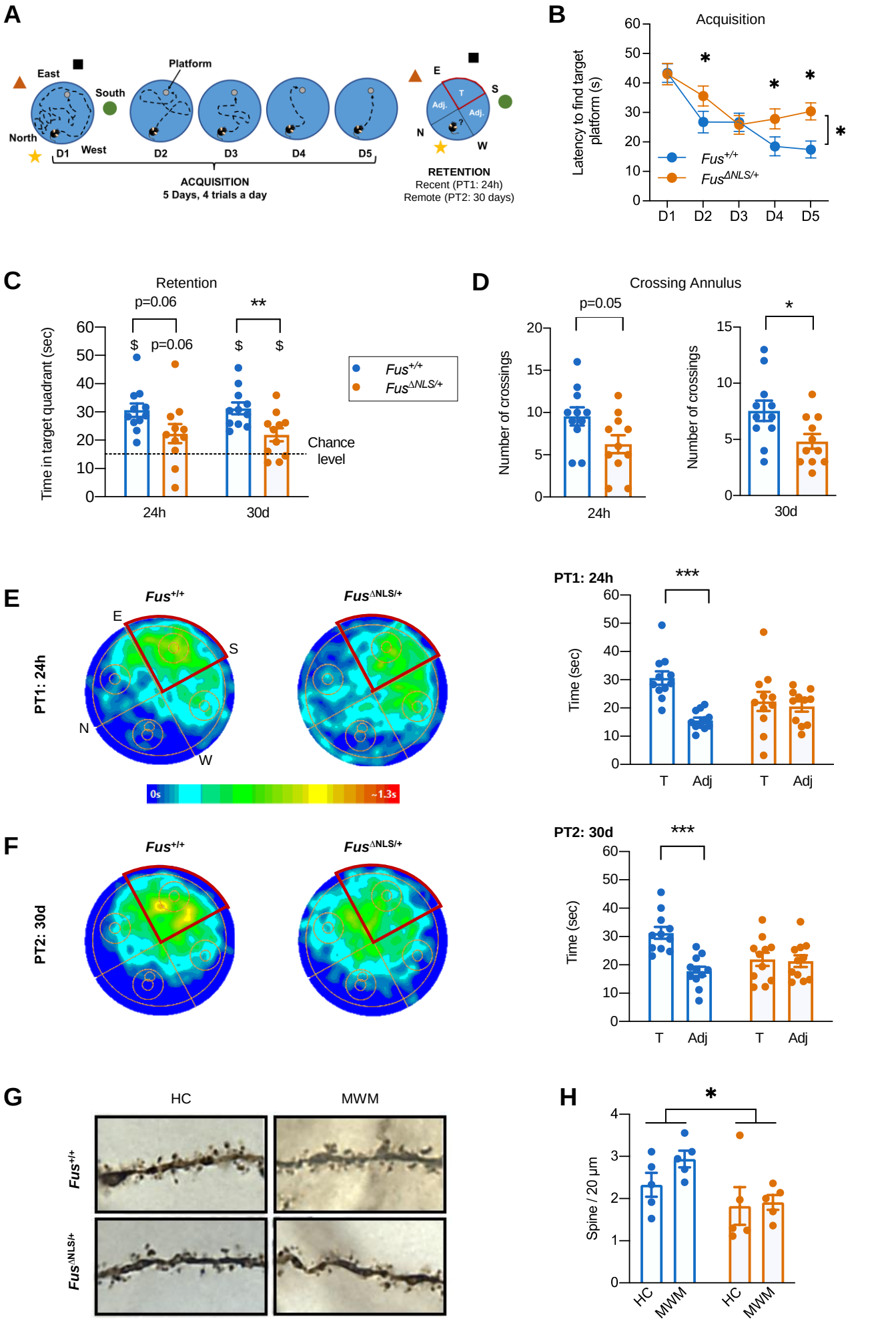
A
East
South
North
West
D1
Platform
D2
D3
D4
D5
ACQUISITION
5 Days, 4 trials a day
E
S
W
N
T
Adj.
Adj.
?
RETENTION
Recent (PT1: 24h)
Remote (PT2: 30 days)
B
Acquisition
Latency to find target platform (s)
Fus+/+
FusΔNLS/+
D1
D2
D3
D4
D5
C
Retention
p=0.06
**
$
p=0.06
$
$
Time in target quadrant (sec)
Chance level
24h
30d
D
Crossing Annulus
p=0.05
*
Number of crossings
24h
30d
E
PT1: 24h
Fus+/+
FusΔNLS/+
0s
~1.3s
***
Time (sec)
T
Adj
F
PT2: 30d
G
HC
MWM
H
Spine / 20 µm